공학석사 학위논문

과냉 조건에 따른 비등 기포의 거동 및 유동장 특성

Analysis on the bubble dynamics and induced liquid flow in a subcooled nucleate pool boiling

2021년 8월

서울대학교 대학원

기계항공공학부

김 현 섭

과냉 조건에 따른 비등 기포의 거동 및 유동장 특성

Analysis on the bubble dynamics and induced liquid flow in a subcooled nucleate pool boiling

지도 교수 박 형 민

이 논문을 공학석사 학위논문으로 제출함
2021 년 4 월

서울대학교 대학원
기계공학부
김현섭

김현섭의 공학석사 학위논문을 인준함
2021 년 6 월

위 원 장 _____ 김호영

부위원장 _____ 박형민

위 원 _____ 황원태

Abstract

In the present study, we experimentally analyze the evolution of vapor bubble dynamics and subsequent bubble-induced flow, produced in a subcooled nucleate pool boiling condition. The development of vapor bubble (growth, departure, rise and collapse) is highly dependent on the subcooled temperature (ΔT_{sub}). Varying the subcooled condition (ΔT_{sub} = 2-15℃), the temporal variation of bubble structure and corresponding flow field of surrounding liquid are measured simultaneously using the high-speed two-phase particle image velocimetry. With growing subcooled temperature, bubble departure diameter (d_d) and bubble growth time (t_g) tend to exponentially decrease. In a less subcooled condition (ΔT_{sub} < 8℃), the bubble continuously grows until departure, while the bubble begins to shrink (condensate) before departing from the wall, in a highly subcooled condition (ΔT_{sub} ≥ 8℃). Based on the heat transfer mechanisms influencing the bubble growth, we develop the bubble growth model available in the subcooled pool boiling condition. The departing bubble in a less subcooled condition (2.5-3.1mm in size) vertically rises with a significant shape deformation influenced by the governing effect of liquid inertial force, and shrinks slowly (low condensation rate). In a highly subcooled condition, however, the smaller bubble (1.5-2.2mm) is detached from the wall, and rapidly dissipates by means of high condensation rate. The rising velocity and aspect ratio of the bubble in the less subcooled condition fluctuate following the deformation of bubble structure. The departing bubble in a highly subcooled liquid is gradually accelerated and flattened until the complete dissipation. Counter-rotating vortical structure induced

around a rising bubble is produced stronger in a less subcooled liquid, and convected further from the wall than the cases of the highly subcooled liquid.

Keyword : Subcooled pool boiling, boiling heat transfer, bubble-induced flow, vapor bubble dynamics, Two-phase particle image velocimetry

Student Number : 2019-23495

Table of Contents

List of Figures

Chapter 1

Introduction

In a gas−liquid two−phase flow, the dynamical characteristics (e.g., rising motion and deformation) of gas bubble in liquid involves a very complicating interaction between two phases, which sometimes results in the modulation of liquid−phase flow characteristics (Kim et al., 2016). While there are many relevant engineering problems like cavitation and aeration, boiling phenomenon would be considered as one of difficult problems to understand and control owing to the additional dependency on thermal interaction (Shoji, 2004). Since the boiling phenomenon is widely considered in engineering applications such as a heat pump, nuclear reactor, and electric battery cooling due to the significant latent heat of evaporation accompanied (Tong and Tang, 1997), there have been a lot of studies to measure and predict the underlying physics (Judd and Hwang, 1976; Yabuki and Nakabeppu, 2014). Depending on the existence of forced convective flow, the boiling phenomenon is classified as flow boiling and pool boiling, and each type of boiling shows different dynamical characteristics. Examination for macroscale flow field around bubble is more reasonable in static condition, since forced convective flow causes additional unsteadiness and inhomogeneity in flow field. To understand independent effect of subcooled temperature on vapor bubble and two phase interaction, investigation for pool boiling is performed in this study.

As is well understood, nucleate boiling occurs when a liquid layer on the surface is sufficiently heated above the critical temperature. After nucleation, the vapor bubble rapidly grows in a hemispherical

structure while pushing the surrounding liquid in a radial direction. At early period of the bubble growth, a significant amount of thermal energy is transferred by the evaporation of microlayer which exists between the bubble base and heater surface (Cooper, 1969). The thermal energy for boiling bubble is also transferred by heat diffusion through the superheated liquid layer developed above the heater surface (Van Stralen, 1966; Narayan et al., 2018). With explosive bubble growth, the surface of bubble attached to the wall gradually shrink, while the buoyancy becomes stronger which induces the bubble departure. A vortical structure develops around the departing bubble and agitates the quiescent liquids (turbulence), which results in the additional heat transfer from the wall (Transient conduction) (Kim, 2009). The pair of vortical liquid flow further induces the heat transfer to the surrounding liquid, while rising vertically (Micro-convection). The applications of boiling phenomena mentioned above, on the other hand, requires us to predict the boiling heat transfer coefficient and critical heat flux (CHF), and thus it is emphasized to have an accurate information of bubble size that characterizes the scale of transient turbulent motion of surrounding liquid (Jaikumar and Kandlikar, 2016).

Temporal evolution of vapor bubble until its lifetime and induced flow field of surrounding liquid shows different characteristics depending on the degree of subcooling. However, although both experimental and theoretical studies for saturated pool boiling have been widely performed, further research is still required for the dynamics of vapor bubble and bubble induced flow in subcooled condition. For saturated condition, the bubble growth has been predicted based on the simplified Rayleigh-Plesset equation by

equating the heat diffusion (conduction) and evaporation:

$$h_{lv}\rho_v \frac{dR}{dt} = Ck_l \frac{T_o - T_{sat}}{\sqrt{\pi \alpha t}} \quad (1)$$

where T_o and T_{sat} indicates the superheated and saturated temperature of liquid, respectively, and h_{lv}, k_l and α denote latent heat, thermal conductivity and thermal diffusivity of water, respectively (Plesset and Zwick, 1954; Forster and Zuber, 1955). According to Baltis and van der Geld, 2015, the growth of bubble in saturated flow boiling condition can be correlated as $R(t) = a_1(t + a_2)^{0.5}$, showing that the bubble growth is governed by heat diffusion for saturated condition. As introduced above, the previous models predict the bubble growth as $R(t) \sim t^{0.5}$ in a saturated condition, which is not appropriate in subcooled case.

The characteristics of vapor bubble dynamics and induced flow field during the lifetime is clearly different, depending on the subcooled condition. However, as the most of bubble growth models were developed assuming the saturated condition, consideration for the effect of subcooling is necessary to accurately predict the bubble growth in subcooled condition. Especially for industrial technologies such as spray cooling system and bubble jet printing, boiling phenomena often occurs in subcooled condition (Lin and Ponnappan, 2003; Asai, 1989). In these cases, the overall dynamics of nucleated vapor bubble until complete dissipation is strongly dependent on condensation heat transfer which occurs through upper part (cap) of the bubble. With growing subcooled temperature, the maximum bubble size decreases and bubble generation frequency increases (Tolubinsky and Kostanchuk, 1970). Experimentally analyzing the effect of pool temperature on bubble growth using R113 as a working fluid, Kim et al., 2006 confirmed that the thermal energy transferred

via microscale heater is lost to the surrounding liquid by condensation heat transfer through bubble interface. Thus, analytical investigation on the vapor bubble growth is further required in subcooled condition.

Finally, most of qualitative investigations for nucleate pool boiling have been focused on microscopic analysis such as dynamics of microlayer and measurement of evaporation heat transfer, caused by significant contribution of microlayer evaporation on bubble growth (Utaka et al., 2013; Sato and Niceno, 2015; Jung and Kim, 2014). However, transient conduction and micro-convection, which are directly related with the macroscopic dynamics of departing bubble and induced flow structure, are dominant mechanisms for overall heat transfer from the wall (Demiray and Kim, 2004). Moreover, the underlying physics of gas and vapor bubble immersed in liquid is completely different, because condensation continuously occurs through the interface of vapor bubble. While a research for dynamics of air bubble rising in water is widely performed (Bhaga and Weber, 1981; Tripathi et al., 2015), detailed investigation for a vapor bubble rising in water and induced flow field is still required. Compared with the air bubble, vapor bubble in similar size undergoes more intense surface deformation by condensation, which highly increases the drag and added mass force (Prosperetti, 2017). Thus, further examination for vapor bubble dynamics and induced flow field of surrounding liquid is required to understand the effect of turbulent characteristics of bubble induced flow on heat transfer coefficient.

As briefly introduced above, analysis for representative bubble characteristics (e.g., bubble departure diameter and bubble growth time) for subcooled condition is further required and detailed study for temporal development of bubble structure and induced flow has

not been performed sufficiently. Therefore, in the present study, we experimentally investigate the vapor bubble dynamics and subsequent bubble-induced flow depending on the subcooled temperature (2-15℃). To measure the gas- and liquid-phase statistics of a pool-boiled flow simultaneously, we use the high-speed two-phase particle image velocimetry (Lee and Park, 2020; Lindken and Merzkirch, 2002). Depending on the subcooled condition, the temporal variation of bubble structure and the bubble-induced agitation in the bulk water is quantified from the measured data, focusing on the interchange between kinetic energy of bubble-induced liquid stream and bubble itself, leading to the circulation (vortical structure) around the bubble. Also, by modifying the existing model for bubble growth, we suggest an improved model that can predict the bubble size evolution even in highly subcooled pool boiling condition. While most of previous studies on pool-boiled bubble addressed the microscopic phenomena such as the microlayer evaporation, the macroscopic information of vapor bubble dynamics and induced flow field targeted in this study will advance our understanding on the phasic interaction in boiling flows.

Chapter 2

Experimental set-up and procedure

2.1. Subcooled nucleate pool boiling

The experiments are performed in a cubic water tank consisted of an acrylic material (150 mm x 150 mm x 150 mm) (Figure 2.1). A pool boiling bubble is nucleated on a mirror-polished stainless steel plate (SS316, thickness of 0.5 mm, averaged roughness of 0.057μm) which is joule heated on the bottom of water tank, using a DC power supply (EX20-180, ODA). To capture the single bubble dynamics, boiling is induced in the condition of onset of nucleate boiling (ONB) regime, ΔT_{wall} = 4–7°C in this study. Without any artificial structure (e.g., micro cavity) on the heater surface, the location of nucleation site is unpredictable. However, above a site where boiling vigorously occurs, bubbles tend to continuously nucleate on the fixed location. As the magnitude of bubble statistics such as bubble departure diameter and bubble growth time is significantly influenced by the surface condition, the measurements are carried out for a single nucleation point for each dataset. Each dataset is obtained while maintaining the constant wall temperature (ΔT_{wall}) and varying the degree of subcooling (ΔT_{sub}). A temperature of bulk fluid is represented by the value measured by RTD probe located in 30mm above the heater plate, and a temperature of heater surface is measured by RTD sensor. From the raw image, the geometry of bubble is analyzed to calculate equivalent diameter and aspect ratio, as shown in Figure 2.2. Both equivalent diameter (d_{eq}) and aspect ratio (χ) of bubble are calculated as $d_{eq} = (d_h^2 d_v)^{1/3}$ and $\chi = d_h/d_v$,

where d_h and d_v indicate the length of horizontal (major) and vertical (minor) axis of bubble geometry, respectively.

2.2. High-speed two-phase particle image velocimetry

High-speed two-phase particle image velocimetry (PIV) is performed to simultaneously analyze the rising motion of bubble and induced liquid flow field. To capture the images of vapor bubble and surrounding liquid, a high-speed camera (SpeedSense M310, Dantec Dynamics) is used, equipped with 100mm macro lens (Samyang) and orange filter (cut-off length of 570 nm) for blocking the green laser light reflected from the heater surface and bubble. As shown in Figure 2.2, a view plane is illuminated by two light sources with different wavelengths (e.g., LED array, 675nm; Continuous-wave laser, 532nm). For a liquid phase, the seeding particle of PS - FluoRed (size of 1 - 20 μm) is suspended and this fluorescent particle is illuminated by a green-colored continuous-wave (CW) laser (RayPower 5000, Dantec Dynamics) emitting the light (wave length of 607 nm). Stokes number for tracer particle (St_p) is defined as the ratio of particle response time (τ_p) to the characteristic time for surrounding flow (τ_f) and calculated as $St_p = \tau_p/\tau_f = (\rho_p d_p^2/18\mu_f)/t_g \approx 9.8 \times 10^{-4} (\ll 1)$, indicating that the effect of suspended particle on the fluid motion is negligible.

Separation of liquid and gas phase information is progressed using a red-colored LED, located on a backside of the test section. As shown in Figure 2.2, the captured image shows separable brightness of fluorescent particle, background liquid, and vapor bubble, which is adequate for phase separation and PIV analysis. Post image

processing is performed to extract the bubble shadow image, applying a median filter and Sauvola method. By using the median filter which is frequently used to remove noise from the image, the phase boundary becomes smooth and relevant for edge detection. The filtered image is binarized with Sauvola method by which each phase is completely separated. For liquid phase, the image containing tracer particle is further analyzed to obtain the flow field around vapor bubble.

To improve the accuracy of particle image velocimetry, the particle image is processed by image sharpening method. The velocity vectors in liquid phase are evaluated by cross-correlation algorithm using fast Fourier transform (interrogation window of 32 x 32 pixels and 75% overlap). The velocity vector (u_{piv}) is calculated as $u_{piv} = M\Delta s / \Delta t$, where M denotes the magnification factor, Δs is particle displacement and Δt is time separation. Concerning the uncertainty of velocity vectors evaluated by particle image velocimetry, the percentage error of measured values can be estimated, using the relation by Lawson et al., 1999:

$$\delta(u_{piv}) = \sqrt{\delta(\mathrm{M})^2 + \delta(\Delta \mathrm{s})^2 + \delta(\Delta \mathrm{t})^2} \quad (2)$$

Error for the magnification factor is calculated as 0.11%, where the value of M is 27.1 μm/pixel in this study. Particle image displacement error is evaluated as pixel resolution divided by mean distance of particle movement, and estimated as 0.76%. High speed camera operating with its inter-frame time of 500ns is used in this study, offering the error of time separation as 0.25%. Therefore, total uncertainty of velocity vectors measured in this study is estimated to be 0.81%. Uncertainty regarding the bubble statistics such as equivalent bubble diameter and aspect ratio also exists, as the

measured values would vary depending on the choice of threshold index in binarization process. Modifying the threshold values (from 0.2 to 0.4), the percentage variation of bubble equivalent diameter and aspect ratio is less than 1.09% and 1.75%, respectively.

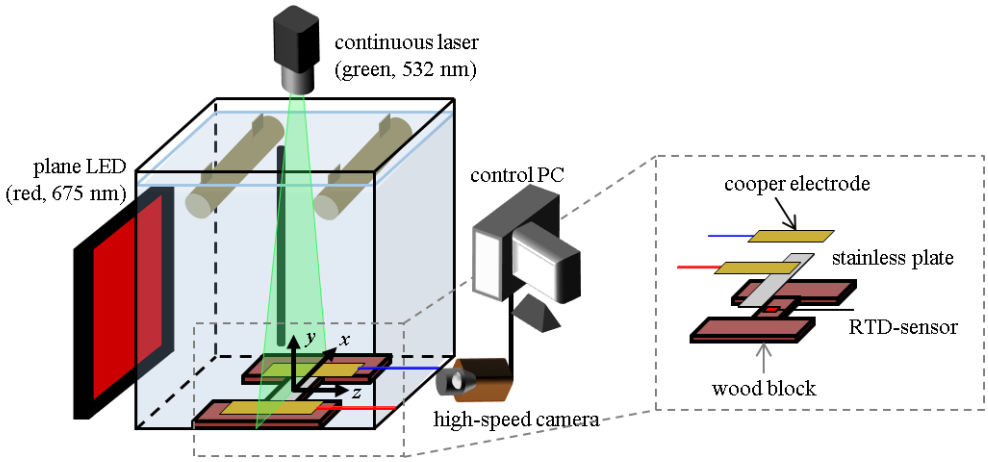

Figure 2.1. Experimental setup for measuring pool boiling flow using two-phase PIV method.

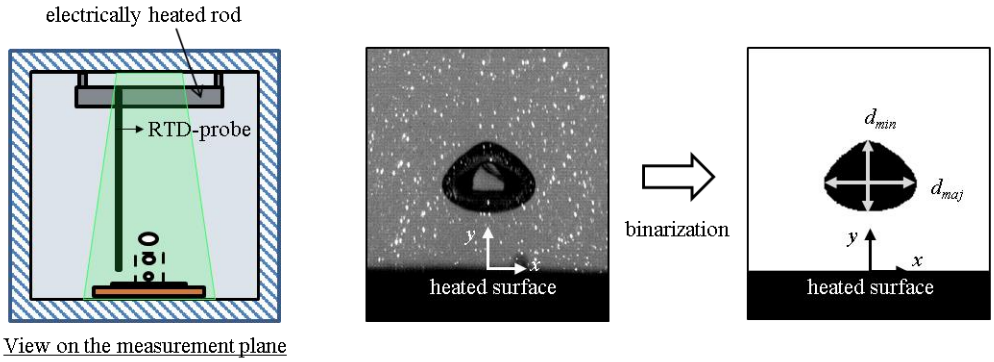

Figure 2.2. Field of view (FOV) in the experimental set-up and representative raw image of the vapor bubble and binarized image .

Chapter 3
Results and discussion

3.1. Lifetime of a subcooled boiling bubble

A temporal evolutions of bubble structure varying the subcooled temperature (ΔT_{sub}) are shown in Figure 3.1. Here, the instance when the bubble is initially distinguished is set as t ~ 0. The normalized time (t^*) is evaluated as the time divided by bubble growth time (t_g) which is defined as an elapsed time when the bubble departs from the heater wall. As shown in the figure, the characteristics (deformation and shape) is clearly different, which is dependent on the degree of subcooled temperature (ΔT_{sub}).

In a less subcooled water (ΔT_{sub} < 8°C), the bubble size becomes greater because the condensation rate is relatively small. And the detached bubble rises upward for a longer distance while shrinking slowly (Figures 3.1). The structure of bubbles moving in a less subcooled water show the significant shape deformation, owing to the larger bubble size (liquid inertia becomes dominant than surface tension). When bubble is detached from the surface (t^* = 1.0), the bubble has a balloon-shaped structure as the base of bubble was attached downward by surface tension. However, as the rear of bubble rapidly shrinks by the interfacial tension, the bubble tends to have an oblate structure. Pulled by the retracting motion of bubble base, a liquid stream in upward direction is induced, which forces the bubble to be accelerated upward after the upper surface of bubble is

bulged up most ($t^* = 1.63$). When the bubble becomes flattened to the most at $t^* \sim 3.0$ (e.g., aspect ratio becomes maximum), the drastic transition of bubble shape occurs from oblate ellipsoidal disk to the spherical cap structure, because the bubble tends to have minimum interfacial area as the surface tension becomes greater for shrinking vapor bubble. Until the complete dissipation, the bubble repeats to be accelerated and decelerated by the movement of vorticity field which was previously induced by rising bubble. In a less subcooled condition, bubble rises upward for approximately more than $3.5 t_g$ before complete condensation.

In a highly subcooled water ($\Delta T_{sub} \geq 8$°C), on the other hand, the smaller bubble is detached from the wall than less subcooled condition (Figures 3.1). Because of the higher condensation rate, the vapor bubble in highly subcooled condition rapidly shrinks into the bulk water. The bubble rising in a highly subcooled water also shows the surface deformation induced by liquid inertia. However, owing to the fast shrinkage of bubble by the intense condensation, the bubble rapidly disappears (its lifetime is about $2.0 t_g$) maintaining a flattened shape.

The departure phenomenon of a vapor bubble is not sufficient to be simply demonstrated with a balance of forces (surface tension and buoyancy). The influence of temperature condition around the bubble and surface condition of heating wall (wettability and roughness) should be considered for determining bubble departure. Bubble growth time (t_g) and bubble departure diameter (d_d) are important boiling bubble parameters, which are shown in Figure 3.2 varying the subcooled temperature (ΔT_{sub}), together with the available data in the literature. These values are directly concerned with representative

bubble size which determines the magnitude of bubble-induced flow and heat transfer caused by surrounding flow structure. With increasing subcooled temperature (ΔT_{sub}), both bubble growth time and bubble departure diameter exponentially decrease independent of T_{wall}. As bubble growth time becomes shorter, the bubble gains less thermal energy required for its growth, causing the smaller bubble departure diameter. Tolubinsky and Kostanchuk, 1970 investigated the effect of subcooled temperature on boiling bubble, and they experimentally show that the maximum diameter of bubble decreases with increasing subcooled temperature (ΔT_{sub} = 5 – 60°C). Goel et al., 2017 performed the boiling experiments using the copper rods as a heater, and they showed that bubble size decrease with the growing ΔT_{sub} and ΔT_{wall}. However, in this study, the influence of wall temperature on the bubble growth time and bubble departure diameter is not noticeable in onset of nucleate boiling (ONB) regime. More important parameter determining the bubble size seems to be the surface characteristics of nucleation point, and we obtained each dataset while maintaining the wall superheat and fixing the nucleation site.

From the viewpoint of bubble dynamics, the bubble will depart from the surface when the buoyancy force exceeds the adhesive surface tension; however, the contribution of the subcooled temperature on bubble departure could not be simply understood by the balance of buoyancy force and surface tension. Griffith, 1958 theoretically studied the bubble growth rates of a boiling bubble and explained that among the several possibilities causing the bubble departure (e.g., aerodynamic lift force and rebound of compression of growing bubble), the influence of liquid inertia around the growing bubble is

dominant. It was explained that the initial bubble growth rate (after nucleation) is quite high such that the surrounding liquid is pushed outward abruptly with a higher velocity (see Figure 3.12). As the growing bubble gradually contacts the colder liquid, the growth rate of bubble rapidly drops and the liquid pushed by the growing bubble is decelerated. Ahmadi et al., 2012 experimentally studied the dynamics of a subcooled flow boiling bubble, and arrived at a similar conclusion such that the bubble lift-off is driven by the unsteady growth force, bubble shape deformation, and condensation heat transfer.

In Figure 3.3, we have plotted the temporal development of normalized bubble equivalent diameter ($d_{eq}^{*} = d_{eq}/d_d$), for the selected cases of subcooled temperature, ΔT_{sub} = 2°C, 6°C, 8°C, and 15°C. The equivalent diameter of bubble is normalized by departure diameter (d_d) and presented with the dimensionless time ($t^{*} = t/t_g$). After the departure ($t^{*} > 1.0$), the bubble is condensed continuously and its rate is much faster in highly subcooled conditions ($\Delta T_{sub} \geq 8$°C) (Figure 3.3(a)). The complete dissipation of the bubble occurs at $t^{*} \sim 2.0$ for highly subcooled conditions, while it is delayed to $t^{*} > 3.5$ for less subcooled conditions ($\Delta T_{sub} < 8$°C). We look into the bubble growth trend before the departure ($t^{*} < 1$) in detail, and interestingly, the effect of subcooled temperature is reversed (Figure 3.3(b)). While the bubble grows gradually and departs at the instant of largest bubble size in less subcooled conditions, the bubble begins to shrink (d_{eq}^{*} becomes maximal at $t^{*} < 1.0$) before departure in highly subcooled conditions. For example, the boiling bubble growing in bulk water of ΔT_{sub} = 15°C starts to shrink at $t^{*} \sim 0.8$. That is, the normalized bubble size at $t^{*} < 1.0$ becomes larger with increasing

ΔT_{sub}, which is opposite to the trends after the departure.

Figure 3.4(a) shows the growth rate ($\dot{R} = dR/dt$) of the bubble depending on the subcooled temperature. It shows that the initially higher growth rate rapidly declines right after the bubble emerges, which proceeds faster with increasing ΔT_{sub}. In a higher subcooled condition, the bubble leaves the wall earlier (noted in the figure), because the faster reduction of bubble growth rate induces a stronger liquid inertia dragging the bubble from the surface. After the bubble stops growing ($\dot{R} = 0$), the condensation rate of bubble becomes greater in highly subcooled cases ($\dot{R} < -0.1$ m/s), leading to the shorter lifetime. In Figure 3.4(b), the dimensionless bubble growth rate ($\dot{R}* = (dR/dt)/(d_d/2t_g)$) is compared varying the subcooled condition. In early period of bubble growth ($t^* < 0.5$), interestingly, $\dot{R}*$ of each subcooled condition is collapsed into a single curve, implying that the heat transfer mechanisms governing the bubble growth is similar (i.e., microlayer evaporation and heat diffusion). As the condensation becomes more influential for the growing bubble ($t^* > 0.5$), $\dot{R}*$ in the highly subcooled condition declines more faster than the less subcooled cases, and it drops much drastically after the bubble departure ($t^* > 1.0$). This indicates that the dominant heat transfer mechanism changes depending on the subcooled condition.

This dependency of bubble size evolution on ΔT_{sub} implies that the role of condensation heat transfer is important to understand the subsequent phenomena occurring in a highly subcooled condition. Before the bubble departure, on the other hand, the surface of bubble attached to the wall gradually shrinks, driven by the liquid inertia and buoyant force. Meanwhile, the microlayer gradually evaporates resulting in the complete depletion of microlayer at $t^* \sim 0.65-0.7$ (for

the case of ΔT_{sub} = 3°C) (Jung and Kim, 2015), indicating that the direct heat transfer from the heated surface becomes relatively small at t^* > 0.7. As the influence of microlayer evaporation becomes negligible after its extinction, the growth of the bubble is then governed by the heat diffusion and condensation heat transfer, which are determined by the thermo-fluid condition of surrounding liquid. Since most of the existing theoretical models to describe the growth of a pool boiling bubble on a heated surface did not pay much attention to the competing influences among these (e.g., microlayer evaporation, heat diffusion, condensation, and so on), it was not feasible to be applied to the subcooled boiling problems. As shown in Figure 3.3(b), the conventional bubble growth model, represented as $d_{eq}^* = (t^*)^{0.5}$ (Cooper, 1969; Plesset and Zwick, 1954; Forster and Zuber, 1955) has a limitation to predict the effect of subcooled condition on bubble growth. In next section, we will suggest a new theoretical model to predict the growth of subcooled boiling bubble, by revisiting and improving the existing heat transfer mechanisms based on our findings.

3.2. Bubble growth model for a subcooled pool boiling

The temporal development of vapor bubble is determined by the surrounding thermal conditions, such as heater surface, superheated bulk liquid and subcooled liquid. Representative schematics for the heat sources and sinks around the vapor bubble are shown in Figure 3.5. First of all, micro-sized liquid layer emerges under the base of bubble. Through the evaporation of this microlayer, the significant amount of heat energy (q_{micro}) is transferred to the bubble (Gerardi et al., 2010). Above the heater surface, the superheated liquid layer

develops and the bubble gains the thermal energy by heat diffusion (q_{diff}), required for their growth. In subcooled pool boiling condition, the cap of vapor bubble is immersed in subcooled water where the condensation heat transfer (q_{con}) occurs. On the other hand, the ratio of bubble surface where each condensation and heat diffusion occur is determined by the thermal condition of bulk liquid around the vapor bubble. Based on the existing bubble growth model (Colombo and Fairweather, 2015), we developed the model considering the heat transfer mechanisms introduced above. The bubble growth rate caused by each heat transfer is superposed and the reliability of the model is enhanced by applying two effective ratios for microlayer depletion and thermal condition around bubble.

Firstly, to evaluate the heat transfer by microlayer evaporation (q_{micro}), the initial thickness of the microlayer (δ_o) should be estimated. Because the present set-up is not equipped to measure the dynamics of microlayer, we relied on the existing models. For the initial thickness of microlayer, both empirical and analytical models have been proposed. The analytical model (Cooper and Lloyd, 1969; van Stralen et al., 1975) was suggested by equating the viscous boundary layer flow in microlayer region, which is in the form of $\delta_o = C(\nu t)^{0.5}$. On the other hand, Utaka et al., 2013 experimentally visualized the microlayer dynamics and proposed the empirical model as $\delta_o = 4.4 \times 10^{-3} r_L$ for water, where r_L denotes the distance between nucleation site and the location of measurement. Both analytical and empirical models for initial microlayer thickness show the similar dependency, regarding the bubble growth rate of $R \sim t^{0.5}$, but have a different coefficient (e.g., analytical model predicts thicker δ_o). Among the several variables determining the magnitude of the

coefficient such as working fluid and system pressure, the material of heater surface also should be considered.

While Cooper and Lloyd, 1969 's model (C = 0.8) is based on the analytical approach, most experimental studies visualizing the microlayer dynamics have been performed using a transparent glass substrate as a heater, which has a stronger hydrophilicity than stainless steel plate. According to Gong and Cheng, 2015, the microlayer evaporation is a major heat transfer mechanism in a hydrophilic surface, but the microlayer does not exist on a hydrophobic surface. In present setup, the departing bubble size (d_d = 1−3 mm) predicted by Cooper and Lloyd, 1969 's model is more reasonable than by the correlation of Utaka et al., 2013 (d_d > 5 mm). Based on the initial thickness model of Cooper and Lloyd, thus, the heat transfer by microlayer evaporation is evaluated by equating the heat conduction through the microlayer and its evaporation (Cooper, 1969). The proposed model is one of the most widely used models with respect to the microlayer evaporation (Colombo and Fairweather, 2015; Raj et al., 2017), and is expressed as:

$$\frac{dR(t)}{dt} = \frac{5}{4} Pr^{-0.5} \mathrm{Ja} \left(\frac{\alpha}{t}\right)^{0.5}. \quad (3)$$

Here, the Jakob and Prandtl numbers are defined as $Ja = \rho_l c_{p,l}(T_{wall} - T_{sat})/\rho_v h_{lv}$ and $Pr = c_{p,}\mu_l/k_l$, respectively, where $c_{p,l}$ and μ_l indicates the specific heat at constant pressure and dynamic viscosity of water, respectively. This model explains that the thermal energy is conducted through the microlayer, which is transported as the growth energy of vapor bubble (evaporation heat). Assuming that the fluid properties does not change much with varying pool temperature, the growth rate of bubble predicted by this model is function of time and wall superheat (ΔT_{wall}).

Second, the bubble growth rate governed by the heat diffusion was suggested by Plesset and Zwick, 1954, assuming the growth of spherical bubble in a superheated liquid. As we have introduced in Chapter 1, a simplified Rayleigh−Plesset equation is solved to obtain the bubble growth rate (dR/dt) (neglecting compressibility and viscous effect), and the effect of evaporation is addressed by equating the heat conduction through the superheated layer and heat transfer required for the phase change (e.g., bubble growth). To solve the Rayleigh−Plesset equation, the pressure term is substituted with the temperature term based on the thin thermal boundary layer approximation. The resulting equation is expressed as:

$$\frac{dR(t)}{dt} = \sqrt{\frac{3}{\pi}} k_l (T_{sup} - T_{sat}) \left(\frac{1}{\alpha^{0.5} \rho_v h_{lv}} \right) t^{-0.5}, \quad (4)$$

where T_{sup} denotes the temperature of superheated water, which is represented with the wall temperature (T_{wall}) in the present study. This indicates that the superheated temperature of the wall determines the evaporation rate of bubble induced by heat diffusion through bubble surface.

Finally, Ranz and Marshall, 1952 experimentally investigated the evaporation of water droplets, and proposed the correlation for the evaporation heat transfer induced by convective flow. In the present study, we used the correlation to address the condensation heat transfer, assuming that the present situation has a similar functional dependence of Ranz and Marhsall (Raj et al., 2017; Tu and Yeoh, 2002; Warrier et al., 2002). The corresponding equation is shown as:

$$\frac{dR(t)}{dt} = \frac{h_{con}}{\rho_v h_{lv}} (\Delta T_{sub}), \quad (5)$$

where the condensation heat transfer coefficient (h_{con}) in a natural

convection state is empirically obtained as $h_{con} = k_l(2+0.6Gr^{1/4}Pr^{1/3})/d$, and the Grashof number is defined as $Gr = g\beta\Delta T_{sub}d^3/\nu^2$ with the thermal expansion coefficient (β) and kinematic viscosity (ν). This model dictates that the condensation rate of bubble is determined by natural convective flow induced by temperature difference (ΔT_{sub}) for a given size of bubble. While we tested different mechanisms for evaluating the condensation heat transfer, such as the forced convection by bubble-induced flow and transient conduction, the model predicted by the natural convection showed the best performance.

To consider the collective contributions of each heat transfer mechanism on the bubble growth, we have combined the corresponding models, while introducing two coefficients of the microlayer evaporation effective ratio (α_1) and superheated ratio (α_2). The former indicates the portion of bubble base where the microlayer evaporation dominantly occurs, and the latter represents the portion of bubble surface contacting the superheated region (otherwise it is interacting with the subcooled liquid region) (Figure 3.5). Thus, the subsequent form of the bubble growth model is shown as below.

$$\frac{dR(t)}{dt} = \frac{5\alpha_1}{4}Pr^{-0.5}\mathrm{Ja}\left(\frac{\alpha}{t}\right)^{0.5} + \alpha_2\sqrt{\frac{3}{\pi}}k_l(\Delta T_{wall})\left(\frac{1}{\alpha^{0.5}\rho_v h_{lv}}\right)t^{-0.5} \qquad (6)$$
$$-(1-\alpha_2)\frac{h_{con}}{\rho_v h_{lv}}(\Delta T_{sub}).$$

To apply the Eq. (6), it is necessary to determine the coefficients α_1 and α_2. The effective ratio for the microlayer evaporation (α_1) is defined as the area of bubble base where microlayer exists divided by the total area of bubble base, since the microlayer is gradually evaporated and heat flux through dry-out region is almost negligible (Jung and Kim, 2014; Sato and Niceno, 2017). As the microlayer

evaporation is considered as a major heat source for bubble growth, the microscopic research has been widely performed to examine the geometry and heat transfer characteristics of microlayer. Recently, Jung and Kim, 2014 experimentally measured the distribution of microlayer and heat flow through the heater plate, using shadow interferometry and infrared high speed camera, respectively. They showed that considerable amount of heat is transferred through the microlayer region. Meanwhile, the microlayer begins to be dried out from the center of bubble base, and the heat transfer over this dry-out region is insignificant, since heat transfer accompanying the phase change (e.g., evaporation) does not occur in this area. Demiray and Kim, 2004 also measured the heat transfer under the nucleating bubbles using microscale heater array and observed a low heat transfer region progressively developed from the center of bubble. To accurately predict the bubble growth rate induced by microlayer evaporation, accounting for the effect of microlayer depletion is essentially required. Analyzing the experimental data for temporal development of dry-out region, this area grows almost linearly with time, as shown in Figure 3.6. Here, the depletion time (t_{dep}) is the time taken for the microlayer to disappear completely. It is noted that it was not allowed to measure the microlayer dynamics directly with the present setup, but the collection of previous studies was found to be sufficient to draw a converged correlation. It is further found that the instance when the microlayer is completely depleted is in common approximately $0.65-0.8t_g$ (t_g: bubble growth time) (Demiray and Kim, 2004; Jung and Kim, 2015). Since the microlayer depletion time is proportional to the bubble life time, it is reasonable to non-dimensionalize it with t_g, and the data we have used were adopted

from Jung and Kim, 2015 (see Figure 3.6 therein). In Figure 3.7(a), we have plotted the temporal variation of the diameter of the bubble base (d_{base}), measured from the binarized image (see the inset), normalized by its maximum value, for selected cases of ΔT_{sub} = 2°C, 6°C, 8°C, and 15°C. The experimental data from Duan et al., 2013 were shown together to support our analysis. Based on the data in Figure 3.6, on the other hand, we modeled the temporal development of dry-out region as d_{dry} / $d_{dry.max}$ = t/t_{dep} = t/(0.7t_g) (0 ≤ t ≤ 0.7t_g). Using the measured base diameter and modeled dry-out diameter, effective ratio (α_1) is calculated and shown in Figure 3.7(b). Supporting our approach, all the data including those of Duan et al., 2013 converge to a single curve in the form of $\alpha_1(t)$ = 1−(d_{dry}/d_{base})^2 = 1−(t/t_{dep})^3 = 1−(t/(0.7t_g))^3 (0 ≤ t ≤ 0.7t_g).

Next, we defined the superheated ratio (α_2) as the proportion of bubble surface contacting the superheated bulk liquid, where the heat diffusion (q_{diff}) occurs dominantly. For the upper part of bubble touching the subcooled liquid, the thermal energy is transferred to the surrounding liquid by the condensation heat transfer. To evaluate α_2, we assume the azimuthal perimeter (l_a) of the bubble, which initially grows in a hemispherical shape (Figure 3.5). Then, the ratio of bubble surface in contact with the superheated liquid can be simplified as a ratio to the bubble equivalent diameter (d_{eq}), i.e., α_2 ~ ξl_a /$d_{eq} l_a$ = ξ /d_{eq} (ξ, thickness of superheated liquid layer). To find out ξ, the temperature distribution above the heater plate is required, which was not allowed with the present setup, thus, we estimated it based on the thermal boundary layer theory. In an isolated regime of pool boiling, it is reasonable to assume that the natural convection occurs (Cho and Wang, 2019). While the effect of preceding bubble

on the wall condition is considered to be not substantial, as we explained above, however, to address the effect of the bubble-induced agitation in the liquid, we used the empirical correlation for the turbulent natural convective boundary layer by Kays and Crawford, 1993: $\delta_t = 7.14(\nu\alpha/g\beta\Delta T)^{1/3}$ (where $\Delta T = T_{wall} - T_\infty$). In Figure 3.8(a), the estimated temperature distribution (for the case of ΔT_{sub} = 8°C and ΔT_{wall} = 4°C) in vertical direction is shown. Here, the distance from the wall to the position of T = 100°C is set to be ξ. Based on the estimated δ_t and ξ, the superheated ratio of departing bubble (ξ/d_d) is obtained for all of the considered wall temperatures and subcooled conditions (Figure 3.8(b)), which shows no apparent tendency. This is because both bubble size (d_d) and superheated layer thickness (ξ) have a similar, but not following the same mathematical correlation, dependency on the subcooled temperature and wall superheat; they increase (decrease) with higher wall superheat (subcooling). Considering the bubble size dependency on surface condition, thus, we assumed it to be constant as an averaged value of $\xi/d_d \simeq 0.11$. As the bubble size can be evaluated as $d_{eq} = d_d(t/t_g)^{0.5}$, the superheated ratio (α_2) becomes a time dependent parameter, as shown in Figure 3.9, which is expressed as $\alpha_2(t) = \xi/d_{eq}(t) = 0.11(t/t_g)^{-0.5}$ (by definition we set α_2 = 1.0 when it is calculated to be larger than 1.0).

Collecting the relations for $\alpha_1(t)$ and $\alpha_2(t)$, the final form of the present bubble growth model is expressed as:

$$\frac{dR(t)}{dt} = \frac{5\alpha_1(t)}{4} Pr^{-0.5}\mathrm{Ja}\left(\frac{\alpha}{t}\right)^{0.5} + \alpha_2(t)\sqrt{\frac{3}{\pi}}k_l(\Delta T_{wall})\left(\frac{1}{\alpha^{0.5}\rho_v h_{lv}}\right)t^{-0.5} \quad (7)$$
$$-[1-\alpha_2(t)]\frac{\Delta T_{sub}k_l}{\rho_v h_{lv} d}(2 + 0.6Gr^{1/4}Pr^{1/3}),$$

where $\alpha_1(t) = 1-(t/(0.7t_g))^3$ (up to $t = 0.7t_g$) and $\alpha_2(t) = 0.11(t/t_g)^{-0.5}$.

Thus, the bubble growth rate in the subcooled condition can be predicted using Eq. (7), given the bubble departure characteristics (d_d and t_g) and temperature conditions (ΔT_{sub} and ΔT_{wall}). After the microlayer depletion (assumed as $t > 0.7 t_g$), the first term of Eq. (7) corresponding to the microlayer evaporation becomes zero, and the bubble growth is governed by the heat diffusion and condensation, which are affected by the temperature distribution around the bubble. The accuracy of the present model can be further improved by the detailed analysis (and modeling) of the temperature field around the bubble. We think this will be meaningful as a future work.

To validate the present bubble growth model (Eq. (7)), we have compared the temporal evolution of bubble diameter predicted for different subcooled conditions (ΔT_{sub} = 2℃, 6℃, 8℃, and 15℃) with the measured data (Figure 3.10). In the figure, the predicted bubble diameter is normalized with bubble departure diameter and presented with dimensionless time, to exclude the influence of the surface characteristics (e.g., roughness, micro-cavity) on the size of bubble. As the representative bubble growth models suggested by Foster and Zuber, 1955, Plesset and Zwick, 1953, and Cooper, 1969 predict the bubble growth proportional to square root of time ($d_{eq}^* = (t^*)^{0.5}$), the function is compared together in the figure. Examining the experimental data for each subcooled condition, bubble continuously grows before departure in less subcooled condition (Figure 3.10(a,b)), while bubble growth rate gradually decreases and the bubble starts to shrink after t^* = 0.75-0.85, in highly subcooled condition (Figure 3.10(c,d)). Bubble growth predicted by square root correlation have a limitation to follow the decreasing trend of experimentally obtained bubble growth rate. The gap between the

experimental data and values predicted by square root correlation becomes greater in higher subcooled condition. On the other hand, the proposed model in this study effectively demonstrates the influence of subcooling on the trend of bubble growth, which is contributed by consideration of microlayer depletion and condensation heat transfer. As the influence of microlayer evaporation becomes negligible at $t^* > 0.7$ (microlayer depletion), the bubble growth rate is determined by the temperature condition of bulk liquid around the bubble. While the bubble continuously grows before bubble departure in less subcooled condition where heat diffusion is more dominant than condensation, the bubble begins to shrink before bubble departure in highly subcooled condition where condensation becomes dominant.

To the best of our knowledge, this is the first analytical model that can explain the bubble growth in a subcooled pool boiling condition including the regime of condensation dominated. On the other hand, further discussion on relevancy of condensation model in terms of predicting bubble growth is provided in the following supplements.

We compare different condensation models, i.e., natural convection, forced convection and transient conduction models, to evaluate the condensation term in Eq. (7), and the predicted results are shown in Figure 3.11. In Eq. (7), we selected the natural convective flow around the bubble as an external flow condition, driving the condensation heat transfer. During the bubble growth, the liquid surrounding the bubble is pushed outward, by which the convective heat transfer is induced. On the other hand, for the forced convective heat transfer induced by bubble growth, the empirical correlation developed by Ranz and Marshall, 1952 is tested, following previous

studies (Colombo and Fairweather, 2015; Raj et al., 2017; Tu and Yeoh, 2002; Warrier et al., 2002), which can be expressed as $h_{con} = k_l(2 + 0.6Re_b^{0.5}Pr^{0.3})/d$. Here, the bubble Reynolds number is defined as $Re_b = \rho_l V_{int} d/\mu_l$, and we use the velocity of bubble interface as $V_{int} = dR/dt$.

During the bubble growth, the bubble Reynolds number becomes constant (Forster and Zuber, 1955); it is, for example, $Re_b \simeq 438$ for the case considered in Figure 3.11. Comparing the natural and forced convection models, the bubble growth shows a similar trend in a less subcooled condition (Figure 3.11(a)), where the influence of subcooled liquid is insignificant. However, in a highly subcooled condition (Figure 3.11(b)), the forced convection model overpredicts the condensation of vapor bubble, while both the bubble growth and collapse rate are more accurately predicted by the natural convection. Although the interface of expanding bubble induces the development of liquid flow, the thermal boundary layer surrounding the bubble is also displaced; that is, the relative movement of liquid to the bubble is not substantial. Thus, it is reasonable to use the natural convection as a source of convective condensation in the present case. We also tested the transient conduction as a condensation mechanism. The equation for bubble collapse rate is obtained by solving the transient conduction equation and energy balance equation on the bubble surface. According to Zuber, 1961, the transient conduction model is expressed as $h_{lv}\rho_v \frac{dR}{dt} = -\frac{\pi}{2} k_l \frac{T_{sat}-T_\infty}{\sqrt{\pi a t}}$, and the bubble collapse rate is considerable during the initial growth phase and tends to become less effective later until the bubble departure. In Figure 3.11, it is shown that the transient conduction model does not match the experimental data well. Since the bubble is submerged in the superheated liquid in

the early period of bubble growth, at which the condensation does not occur, the transient conduction model with a higher growth or collapse rate in the initial stage ($dR/dt \sim t^{-0.5}$) is not suitable for the condensation term. Finally, the limited prediction by the simple square root relation ($dR/dt \sim t^{-0.5}$), especially in a highly subcooled condition (Figure 3.11), implies that the heat transfer mechanisms governing the bubble growth and collapse are interacting in a complex manner. In the present study, we have discussed that the microlayer evaporation, heat diffusion, and condensation are the major heat transfer mechanisms for the bubble growth.

3.3. Liquid flow induced by the evolving vapor bubble

Dynamical characteristics of rising vapor bubble is governed by the forces, such like surface tension, liquid inertia, buoyancy, and pressure forces. Investigation on the bubble dynamics and corresponding flow field is of great importance, because these determine the heat and mass transfer of rising bubble (Maeng and Park, 2021). Also, to accurately simulate the multiphasic interaction of boiling bubble, further examination for shape evolution of vapor bubble and induced flow structure should be conducted.

After bubble nucleation, the bubble rapidly grows above the wall and pushes the surrounding liquid.

As shown in Figure 3.12, the liquid flow displaced by the growing bubble decelerates gradually until the bubble departure, owing to the reduction of bubble growth rate (Figure 3.4). Liquid inertial force is induced as the low pressure region develops in front of the bubble which is resulted from the reduction of liquid velocity pushed by growing bubble. The surface of bubble attached to the wall gradually

shrinks forced by the liquid inertial force and increasing buoyant force. At $t \sim 0.5 t_g$, upward flow field emerges beside the bubble base, as the base of bubble is continuously detached from the wall. Bubble finally departs governed by complex interaction of liquid inertial force, buoyant force and upward circulating flow structure.

As the bubble vertically rises driven by buoyant force, upward circulating stream develops in the wake region of bubble and this flow structure induces the surrounding fresh water to replace the superheated water having existed in thermal boundary layer, and this mechanism of heat transfer is called transient conduction (Mikic and Rohsenow, 1969). To compare the bubble induced flow structure concerned with transient conduction, the flow field around bubble at $t = t_g + 0.4\ msec$ is presented in Figure 3.13. The size of the vortical stream around bubble tends to increase with the magnitude of departing bubble. As can be expected, larger bubble in less subcooled condition seems to replace more amount of superheated water in thermal boundary layer with surrounding subcooled water (Figure 3.13 (a,b)). However, in a highly subcooled condition, the bubble-induced flow in the wake region becomes faster, which is caused by the shorter distance between the counter-rotating vortices (Figure 3.13 (c,d)). As the growth rate of bubble drops more rapidly in higher subcooled condition, liquid inertial force induced by pressure gradient becomes stronger which is presented as high velocity field in the rear of bubble. In other words, larger circulating flow structure develops in less subcooled condition, while the bubble induced flow developed in the rear of bubble is faster in highly subcooled condition.

In a less subcooled condition ($\Delta T_{sub} < 8°C$), the rate of condensation is insignificant and bubble departs from the heater surface in large

size, corresponding to the Reynolds and Weber numbers of $Re = \rho_l d_d V_{max}/\mu_l =$ 4800−5400 and $We = \rho_l d_d V_{max}^2/\sigma =$ 14.2−14.5, respectively, based on its departure diameter (d_d) and maximum rise velocity (V_{max}). Here, σ stands for the surface tension and ρ_l and μ_l denotes the density and dynamic viscosity of water. Thus, Bubble rising in less subcooled water undergoes a significant surface deformation, as a liquid inertial force becomes dominant for a large bubble (Figure 3.1). Liquid inertial force induced by bubble deformation repeats to accelerate and decelerate the bubble depending on the direction of induced liquid stream. The rising bubble tends to be gradually flattened while the volume of bubble continuously shrinks by condensation. Further condensed, the bubble becomes flattened to the most and the aspect ratio of bubble radically drops because surface tension becomes dominant for shrunken bubble. This transition of bubble shape from oblate ellipsoidal disk to spherical cap occurs very rapidly, and it causes the collapse of symmetry in bubble structure leading the formation of bubble path instability (Tripathi et al., 2015; Lee and Park, 2017; Ern et al., 2012). The temporal evolution of bubble structure and induced flow field in a less subcooled condition is shown in Figure 3.14 and 3.15 for ΔT_{sub} = 2°C and 6°C, respectively. In Figure 3.16, the time history of bubble aspect ratio and rising velocity is plotted together for comparison.

When a vapor bubble departs from the wall (t^* = 1.0), the base of bubble remains stretched as it was attached to the wall by surface tension before the bubble departure (Figure 3.14(a), 3.15(a)). The balloon−shaped departing bubble tends to become an oblate structure influenced by surface tension acting on the deformed bubble surface (Figure 3.14(b), 3.15(b)). As the bubble base is retracted abruptly

by the interfacial tension, this movement induces the development of rising liquid stream in the wake behind the bubble. Even after becoming a stable oblate shape, the bubble inertially undergoes deformation to be stretched upward by liquid momentum force previously induced by bubble deformation (Figure 3.14(c), 3.15(c)) and this force accelerates the bubble (Figure 3.16(b)). As the bubble is gradually accelerated by the liquid inertia, the counter-rotating vortex pair develops stronger. The downward deformation of bubble surface causes the deceleration of bubble (Figure 3.16(b)), because liquid momentum force driven by bubble deformation is engaged in the opposite direction of bubble movement (Figure 3.14(d), 3.15(d)). Through continuous condensation and surface deformation, the length of minor axis of bubble rapidly shrinks while that of major axis remains almost constant (e.g., aspect ratio of bubble increases) (Figure 3.16(a)). After the bubble is lastly accelerated at $t^* \sim 2.7$ (deformed in a bulged-up shape), it is maximally flattened (the aspect ratio peaks) (Figure 3.14(f), 3.15(f), and 3.16). As the volume of bubble is gradually reduced, the structure of bubble rapidly transforms to spherical cap shape as surface tension becomes dominant for sufficiently shrunken bubble (Figure 3.14(g), 3.15(g)). The magnitude of buoyant force diminishes with persistent condensation of bubble, and kinetic energy of bubble is gradually dissipated by viscous effect of liquid. Meanwhile, through radical transition of bubble shape from oblate ellipsoidal disk to spherical cap shape, break-down of symmetry in bubble structure induces wake instability causing the twist in rising path of bubble. Vortex structure previously developed by bubble-induced flow further remains and assists the bubble to move following the direction of vorticity

convection which is presented as the fluctuation of bubble velocity before dissipation (Figure 3.16(b)). Even after the complete condensation of bubble, the vortex pair continues to rise upward weakened by viscous force (Figure 3.14(h), 3.15(h)).

The dynamics of vapor bubble rising in a highly subcooled water (ΔT_{sub} = 8, 15°C) is more influenced by the significant condensation rate and thus a smaller bubble (Re = 3100−4800 and We = 11.9−17.3) is detached from the wall. In highly subcooled condition, the bubble growth rate drops much faster than the bubble in less subcooled liquid, as shown in Figure 3.4. The more radical decrease of growth rate causes the larger pressure gradient in front of the bubble, and stronger liquid inertial force is induced in this region. As a result, the bubble in highly subcooled condition is detached more frequently, and departing bubble is accelerated faster than a bubble in less subcooled condition. By means of high condensation rate, the transition of bubble morphology occurs quickly and the effect of surface deformation on bubble velocity becomes less significant. In this case, the bubble tends to be flattened gradually and accelerated until the complete condensation. In Figure 3.17, the vapor bubble dynamics and induced flow fields for ΔT_{sub} = 8°C and 15°C are shown, and the corresponding time history of bubble statistics is plotted in Figure 3.18.

At bubble departure (t^* = 1.0), the bubble is detached as a balloon−shaped structure, while the degree of downward stretching is less than the bubble in a less subcooled condition, affected by growing effect of surface tension for smaller bubble. Affected by interfacial tension, the downward stretched bubble tends to become an oblate structure causing the base of bubble to rise rapidly (t^* ~ 1.09). The

fast movement of bubble base (surface deformation) induces the development of upward liquid inertial force in the rear of the bubble. As the kinetic energy of induced liquid stream is transported to the bubble, the bubble velocity begins to increase at the instant when the bubble is maximally deformed upward ($t^* \sim 1.4-1.5$) (Figure 3.18(b)). While being accelerated, the rising bubble becomes flattened with the maximum aspect ratio and rising velocity before the complete dissipation at $t^* \sim 2.0$ (Figure 3.18). As the bubble undergoes a significant condensation with fast rising motion, it dissipates without a noticeable transition of bubble morphology. After the complete dissipation of the vapor bubble, the bubble-induced counter-rotating vortex pair is further dispersed upward for some time, being weakened by the viscous dissipation.

As explained above, the characteristics of the vapor bubble dynamics and bubble statistics can be divided into the less ($\Delta T_{sub} < 8°C$) and highly ($\Delta T_{sub} \geq 8°C$) subcooled regimes. After the departure, the bubble in a highly subcooled condition undergoes more significant condensation, and completely condenses at $t^* \sim 2.0$ while the bubble in a less subcooled condition survives until $t^* > 3.5$. During the relatively longer lifetime, the bubble in a less subcooled condition undergoes an intensive surface deformation, inducing the fluctuation of aspect ratio and bubble velocity (Figure 3.16). However, in a highly subcooled condition, the departing bubble is gradually accelerated after deformed upward ($t^* \sim 1.4-1.5$), and completely condenses in a mostly flattened shape (Figure 3.18).

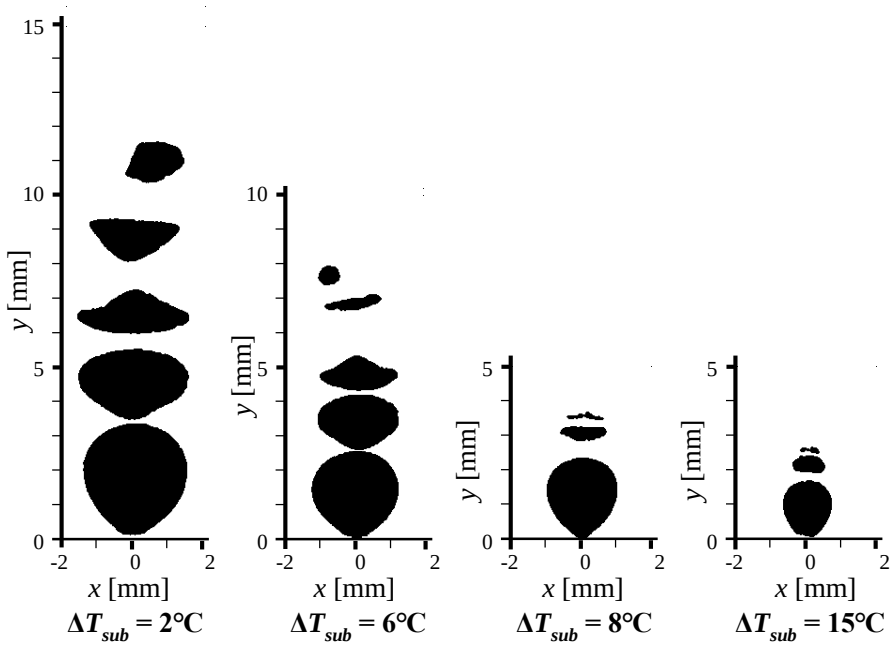

Figure 3.1. Sequential images of pool boiling bubble departing from the heater surface with varying the subcooled temperature (ΔT_{wall} = 4℃).

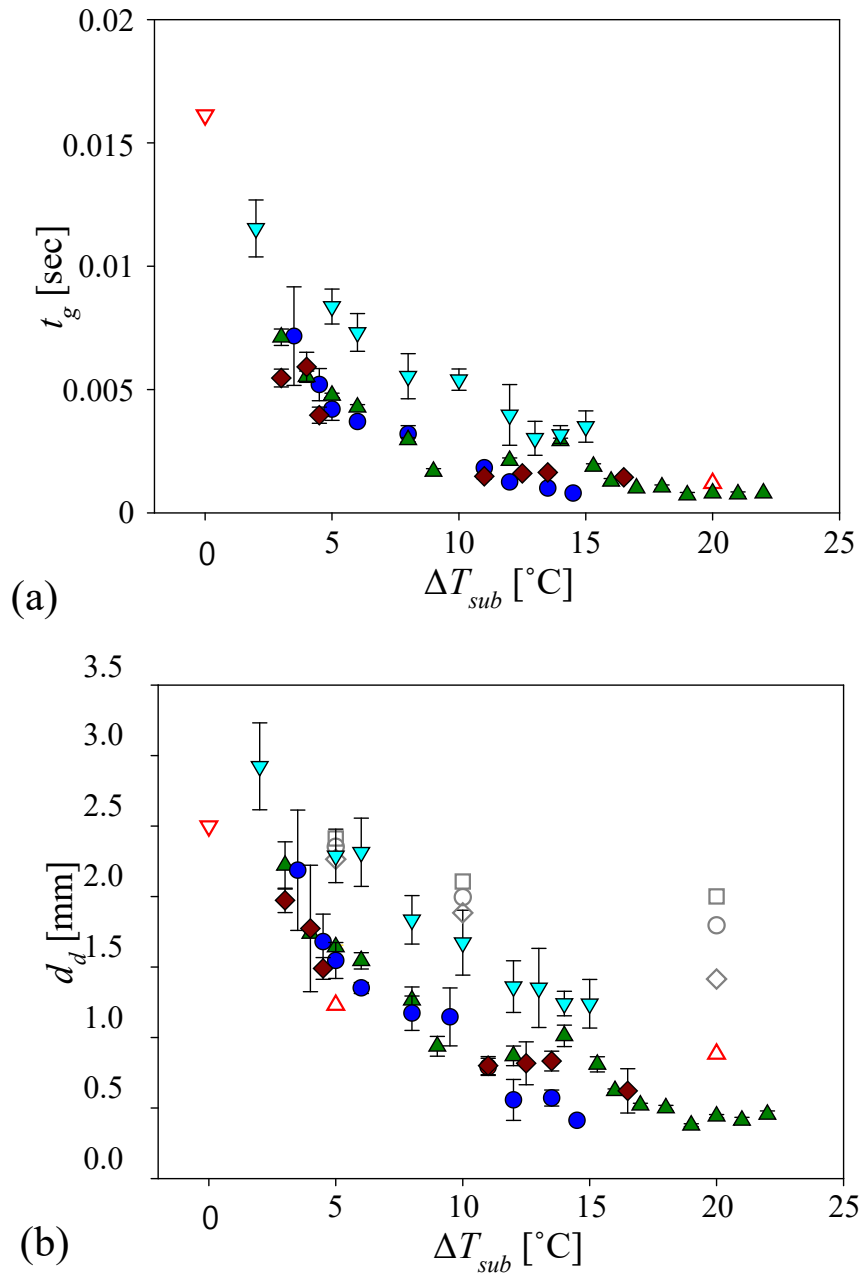

Figure 3.2. Variation of (a) bubble growth time (t_g) and (b) bubble departure diameter (d_d) with ΔT_{sub}. ▼, ΔT_{wall} = 4℃; ●, 5℃; ▲, 6℃; ◆, 7℃ (present study); ▽, Tolubinsky and Ostrovsky, 1966; △, Tolubinsky and Kostanchuk, 1970; □, ΔT_{wall} = 7.5℃; ○, 9.5℃; ◇, 10.5℃ (Goel et al., 2017).

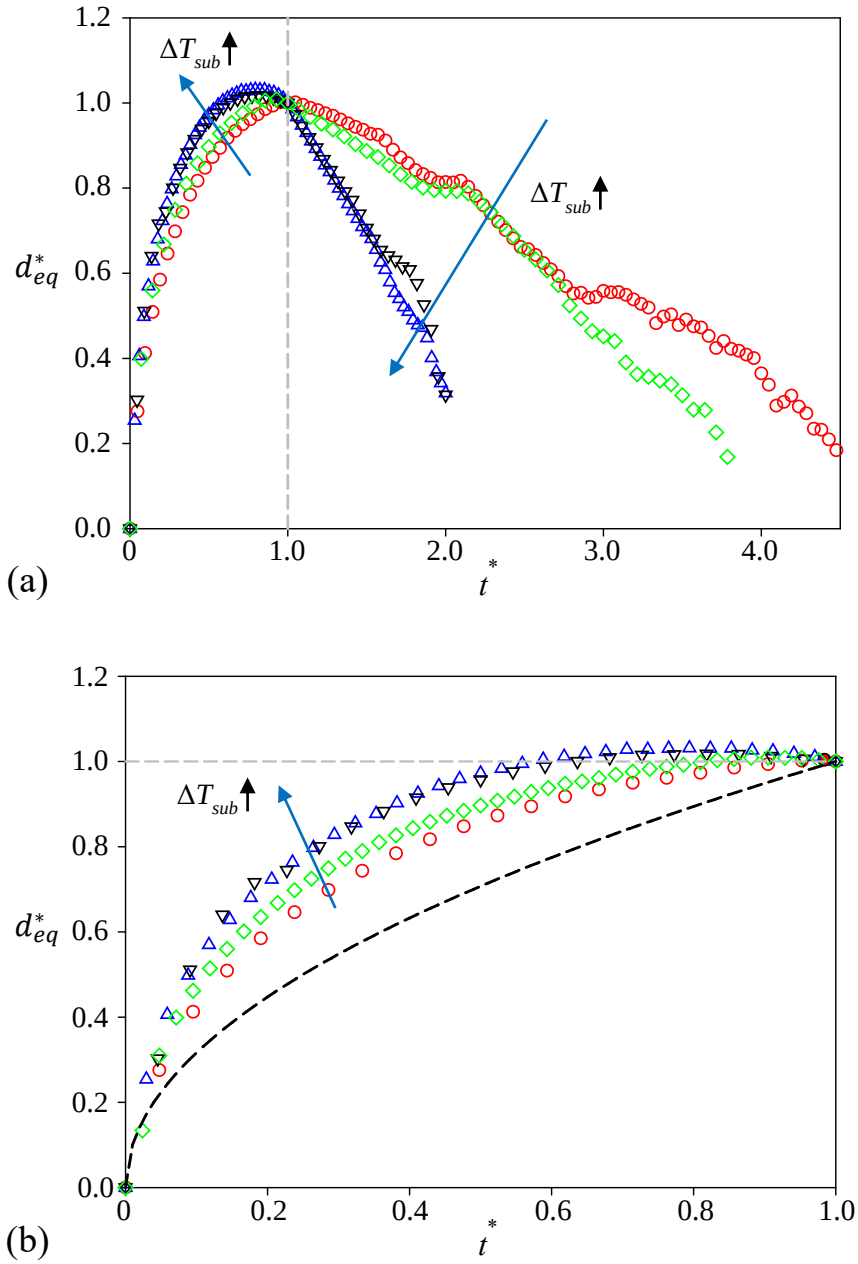

Figure 3.3. Time history of normalized bubble equivalent diameter (d_{eq}^*) until (a) bubble dissipation and (b) bubble departure. ◯, ΔT_{sub} = 2℃; ◇, 6℃; △, 8℃; ▽, 15℃ (present study, ΔT_{wall} = 4℃). In (b), dashed line implies the bubble growth predicted by $d_{eq}^* = (t^*)^{0.5}$ (Forster and Zuber, 1955; Plesset and Zwick, 1953).

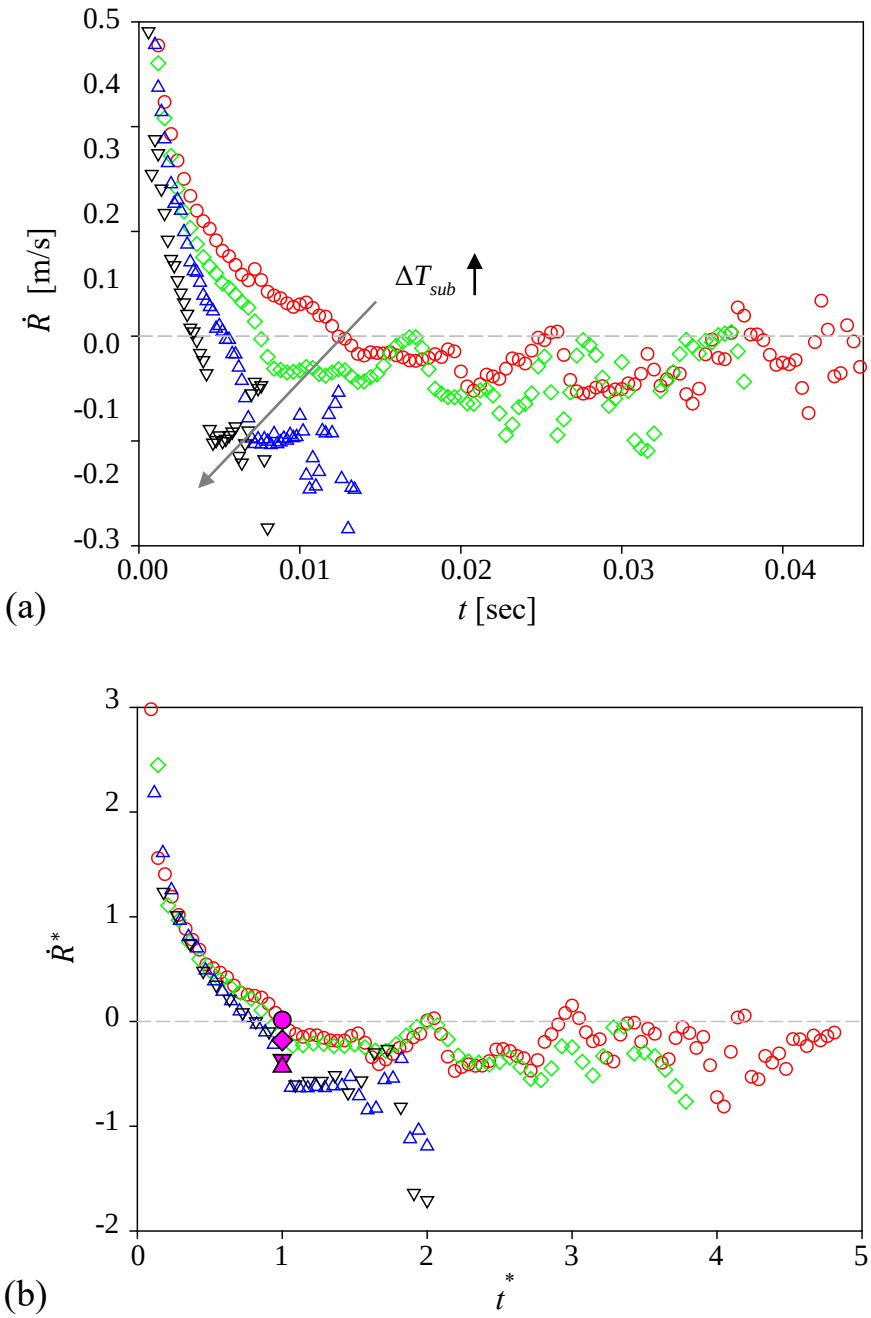

Figure 3.4. Temporal development of (a) bubble growth rate ($\dot{R}$) and (b) normalized bubble growth rate ($\dot{R}^*$). ○, ΔT_{sub} = 2℃; ◇, 6℃; △, 8℃; ▽, 15℃ and ΔT_{wall} = 4℃. Here, the closed symbols denote the instant of bubble departure ($t = t_g$).

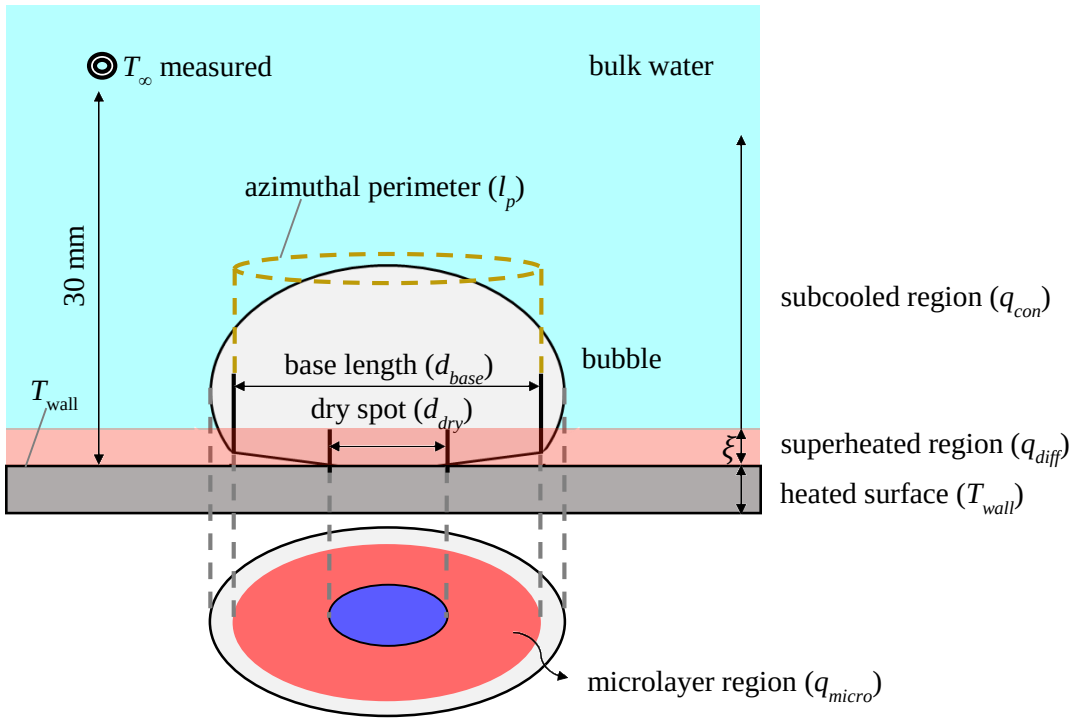

Figure 3.5. Schematic diagram for heat transfer mechanisms contributing to the growth of a bubble in a subcooled nucleate pool boiling.

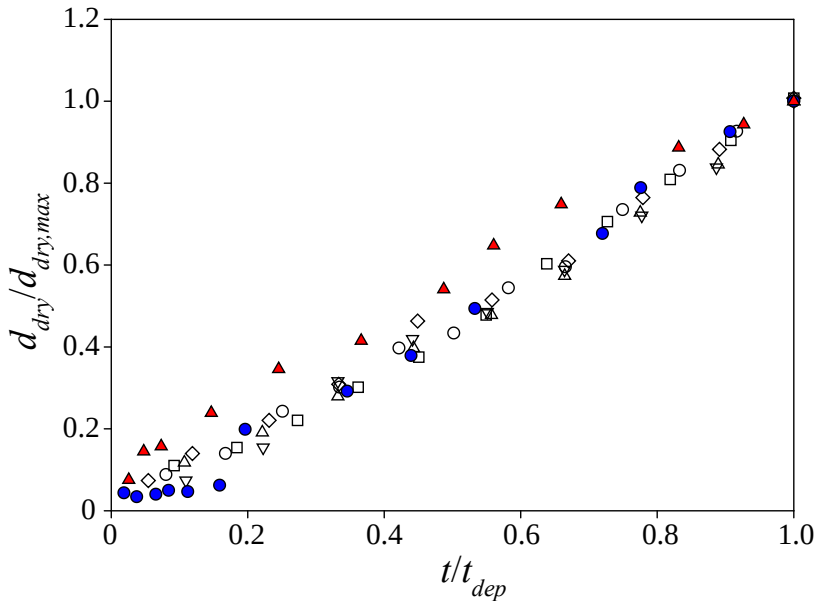

Figure 3.6. Time history of the diameter of dry-out region (normalized by the maximum value): ◯, ▽, ◇, △, Jung and Kim, 2015 (water, ΔT_{sub} = 3℃, sequentially nucleating at the same site); ●, Gao et al., 2013 (ethanol, ΔT_{sub} = 6.1℃); ▲, Chen et al., 2020 (water, ΔT_{sub} = 0℃). Here, t_{dep} is the time taken for the microlayer to be depleted.

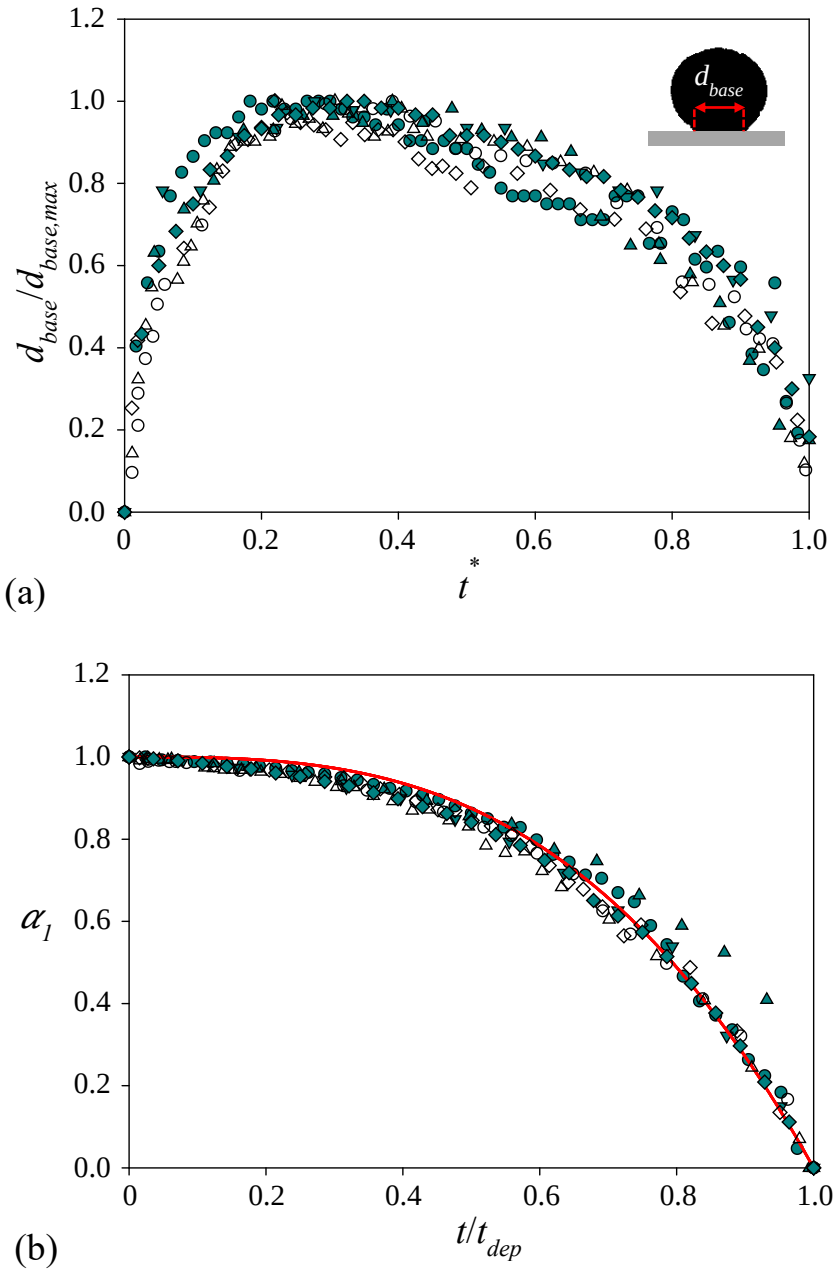

Figure 3.7. Temporal variations of (a) normalized bubble base diameter and (b) microlayer evaporation effective ratio (α_l): ●, ΔT_{sub} = 2℃; ◆, 6℃; ▲, 8℃; ▼, 15℃ (present study, ΔT_{wall} = 4℃); ○, ◇, △, Duan et al., 2013 (ΔT_{sub} = 0.5℃, ΔT_{wall} = 9℃, sequentially nucleating at the same site). In (b), the solid line denotes the model for effective ratio, $\alpha_l = 1 - (t/t_{dep})^3$.

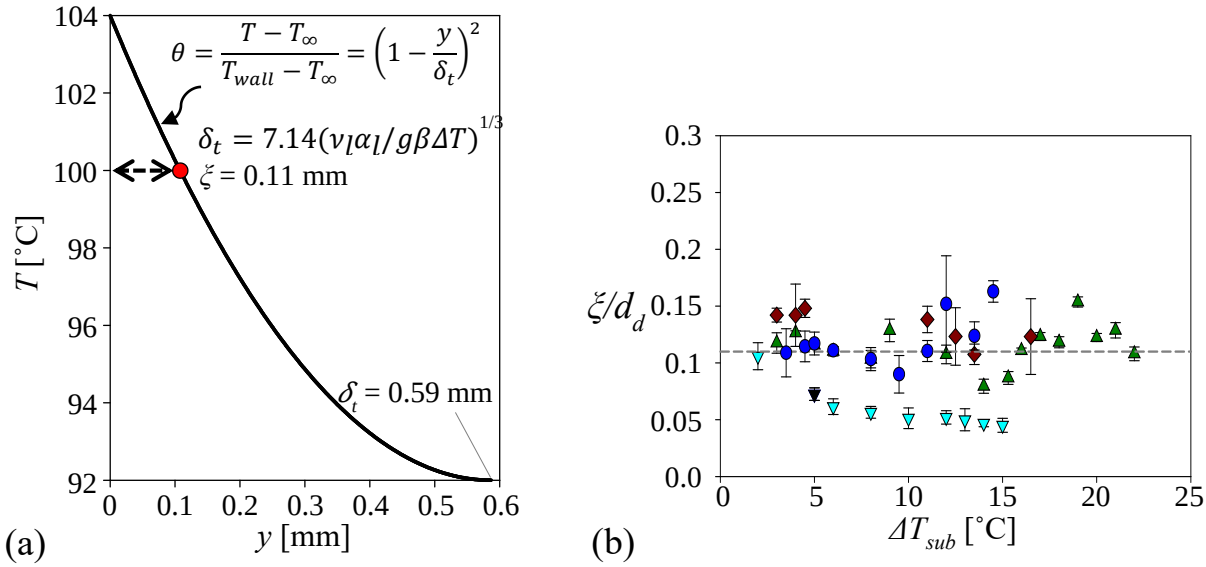

Figure 3.8. (a) Analytically estimated temperature distribution (Kays and Crawford, 1993) above the heated surface (ΔT_{sub} = 8℃, ΔT_{wall} = 4℃). (b) Variations of superheated ratio at bubble departure (ξ/d_d) for different subcooled and wall superheat conditions. ▼, ΔT_{wall} = 4℃; ●, 5℃; ▲, 6℃; ◆, 7℃.

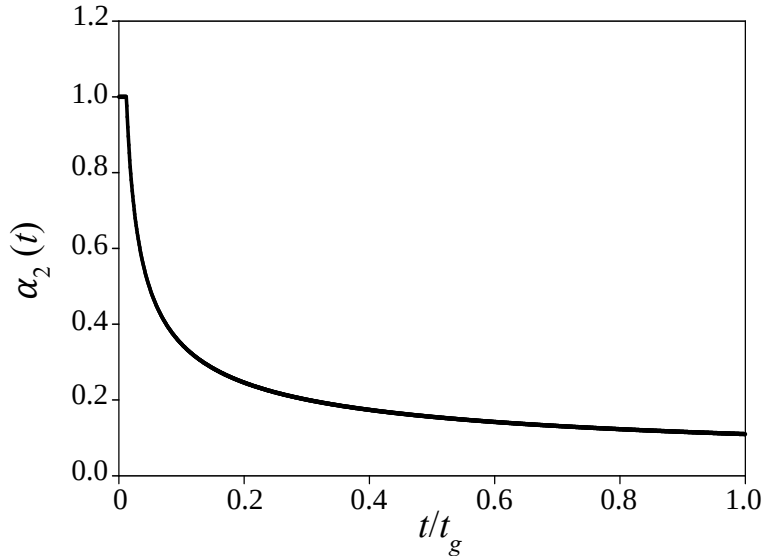

Figure 3.9. Temporal variation of α_2(t) plotted with normalized time (t/t_g).

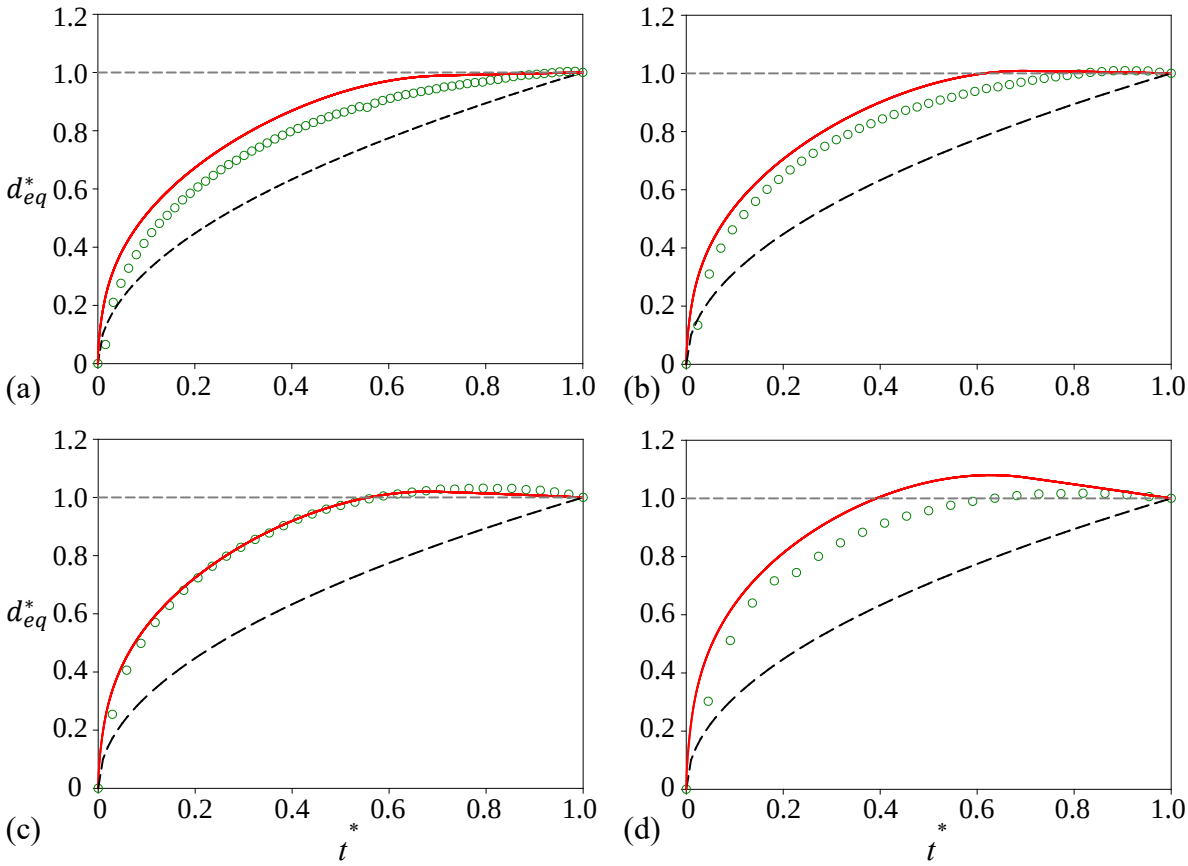

Figure 3.10. Temporal variation of normalized bubble equivalent diameter: (a) ΔT_{sub} = 2℃; (b) 6℃; (c) 8℃; (d) 15℃. ○, experimental data; solid line, prediction by the present model (Eq. (7)); dashed line, square root correlation of $d^*_{eq} = \sqrt{t^*}$ (Plesset and Zwick, 1953; Forster and Zuber, 1955; Cooper, 1969). Here, ΔT_{wall} = 4℃.

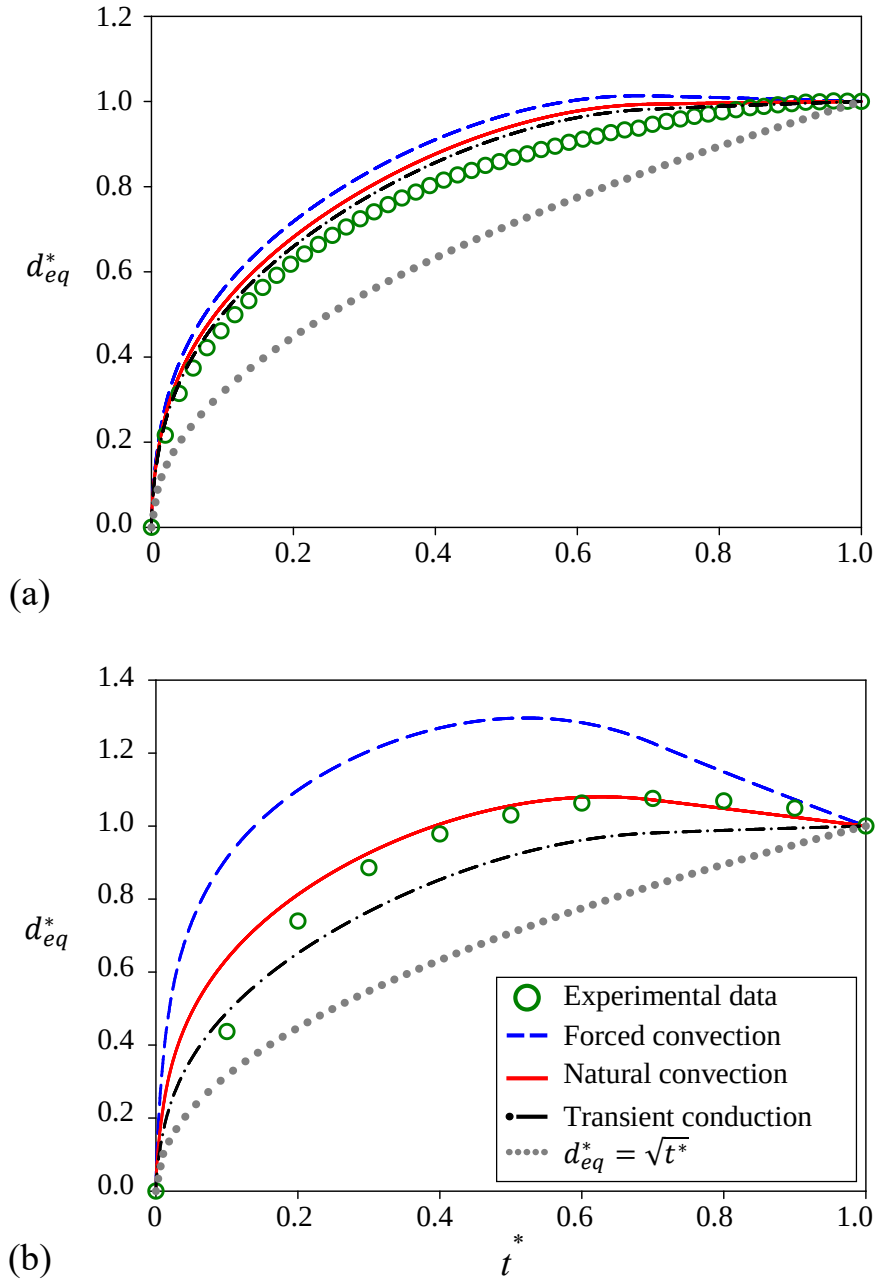

Figure 3.11. Comparison of bubble growth predicted by different models: (a) ΔT_{sub} = 3.5℃; (b) 13.5℃. Here, ΔT_{wall} = 5℃.

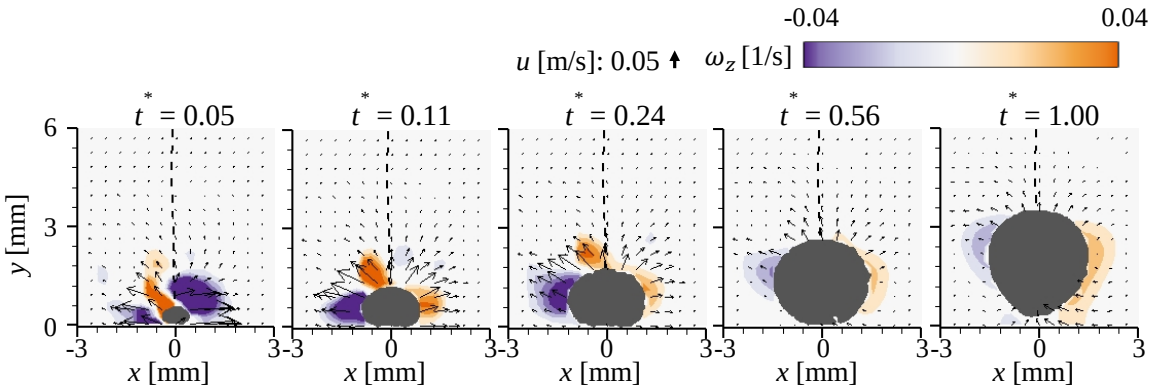

Figure 3.12. Time history of the flow field induced by the growing vapor bubble (before departure) with ΔT_{sub} = 2℃ (ΔT_{wall} = 4℃). The dashed line denotes the rising trajectory of the bubble.

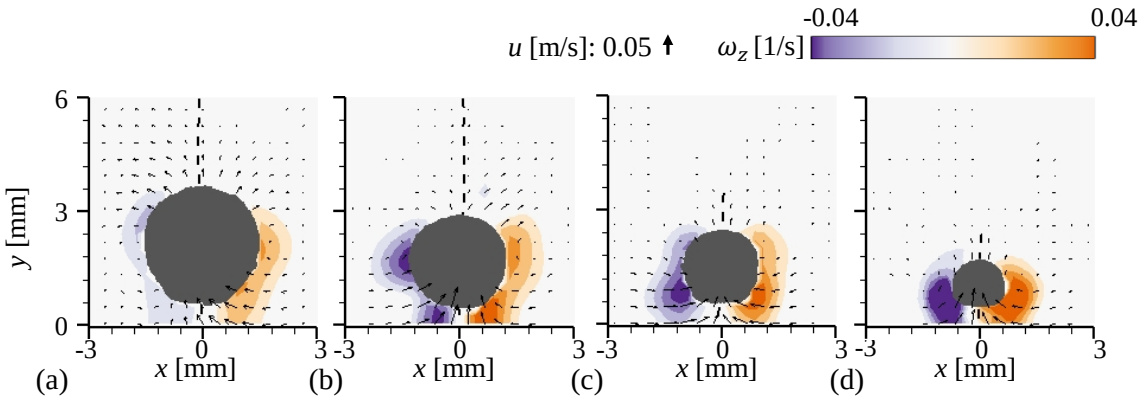

Figure 3.13. Flow field (velocity vectors and spanwise vorticity contour) induced by the subcooled−boiling bubble at the instant ($t = t_g + 0.4\ msec$) of transient conduction heat transfer: (a) ΔT_{sub} = 2℃; (b) 6℃; (c) 8℃; (d) 15℃. Here, ΔT_{wall} = 4℃. The dashed line denotes the rising trajectory of the bubble.

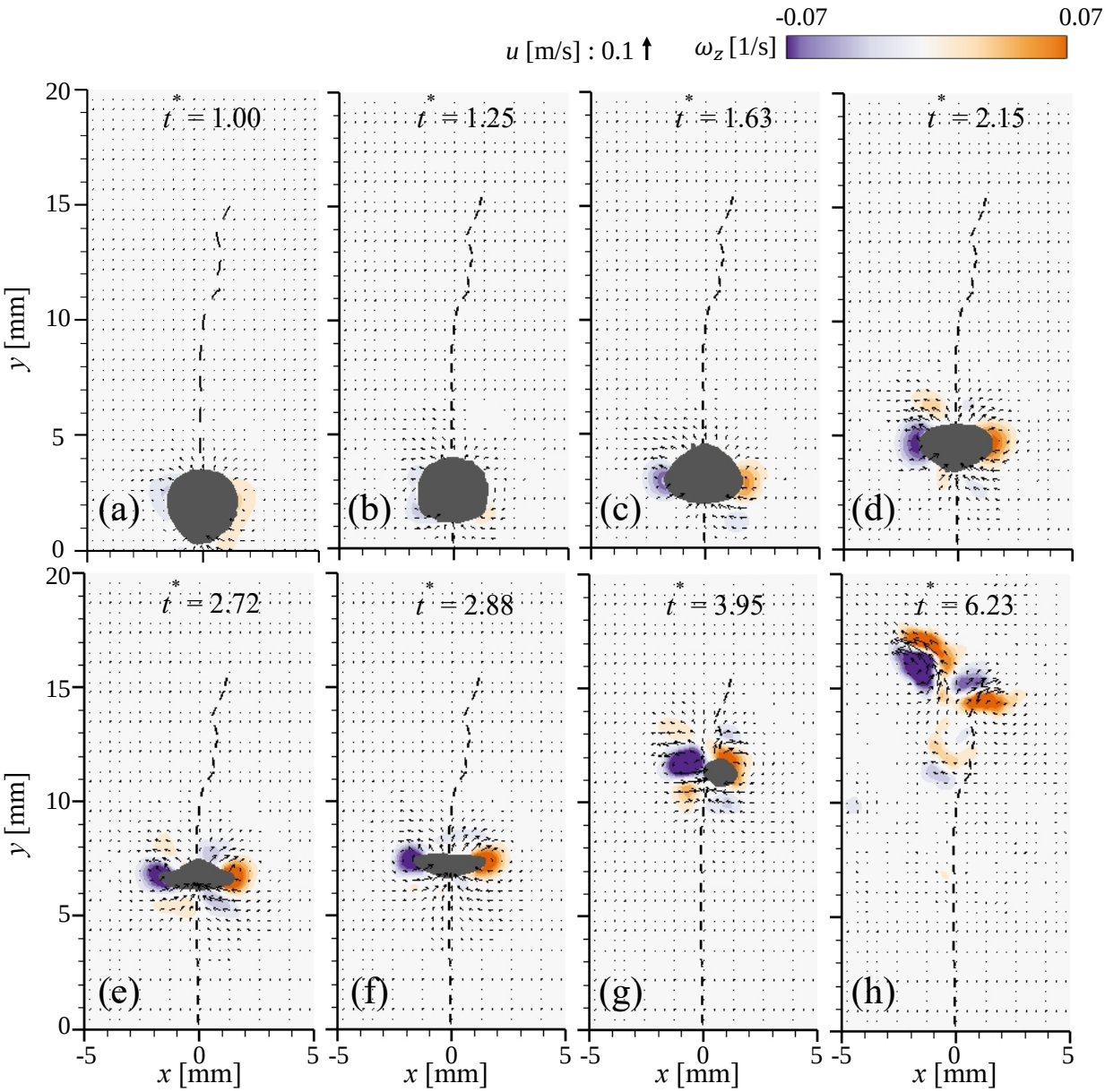

Figure 3.14. Time history of the flow field induced by the rising vapor bubble with ΔT_{sub} = 2℃ (ΔT_{wall} = 4℃). The dashed line denotes the rising trajectory of the bubble.

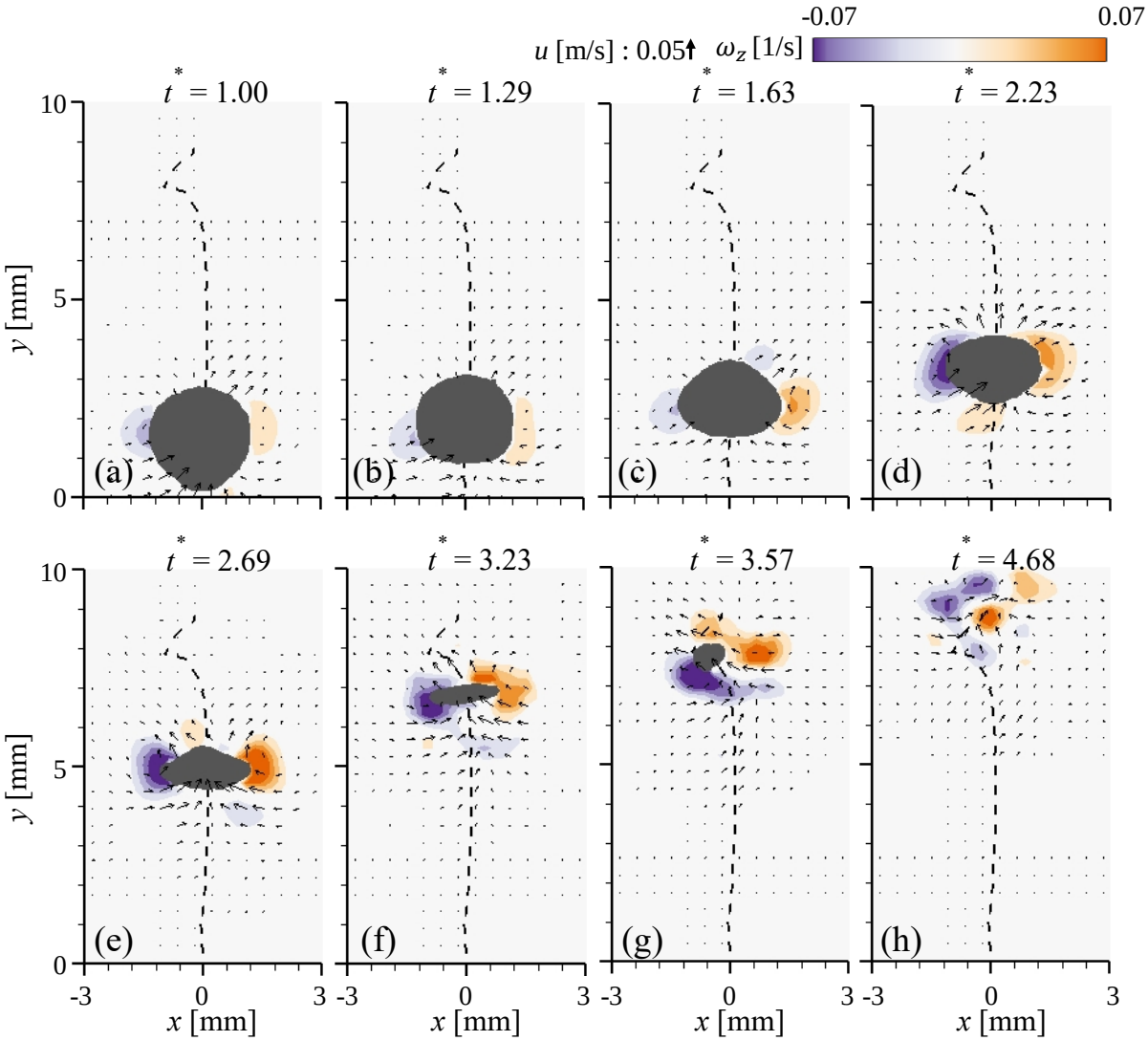

Figure 3.15. Time history of the flow field induced by the rising vapor bubble with ΔT_{sub} = 6℃ (ΔT_{wall} = 4℃). The dashed line denotes the rising trajectory of the bubble.

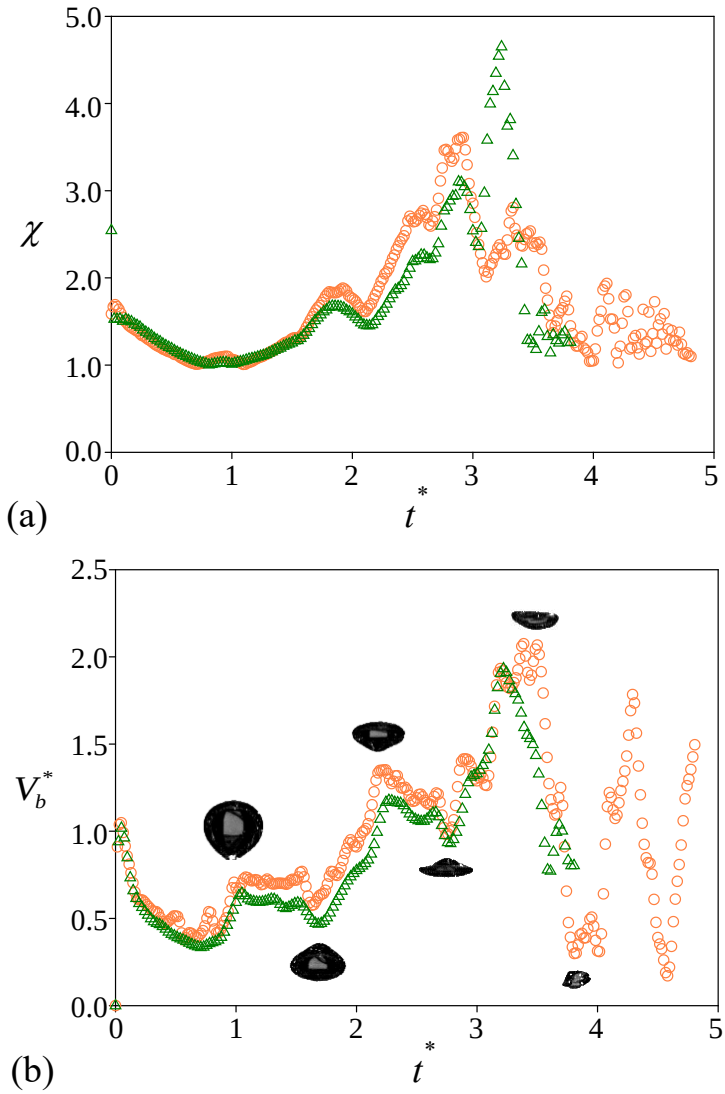

Figure 3.16. Time history of bubble statistics in a less subcooled conditions: (a) bubble aspect ratio (χ); (b) rising velocity ($V_b^* = V_b t_g / d_d$). ○, ΔT_{sub} = 2℃; △, 6℃. Here, ΔT_{wall} = 4℃.

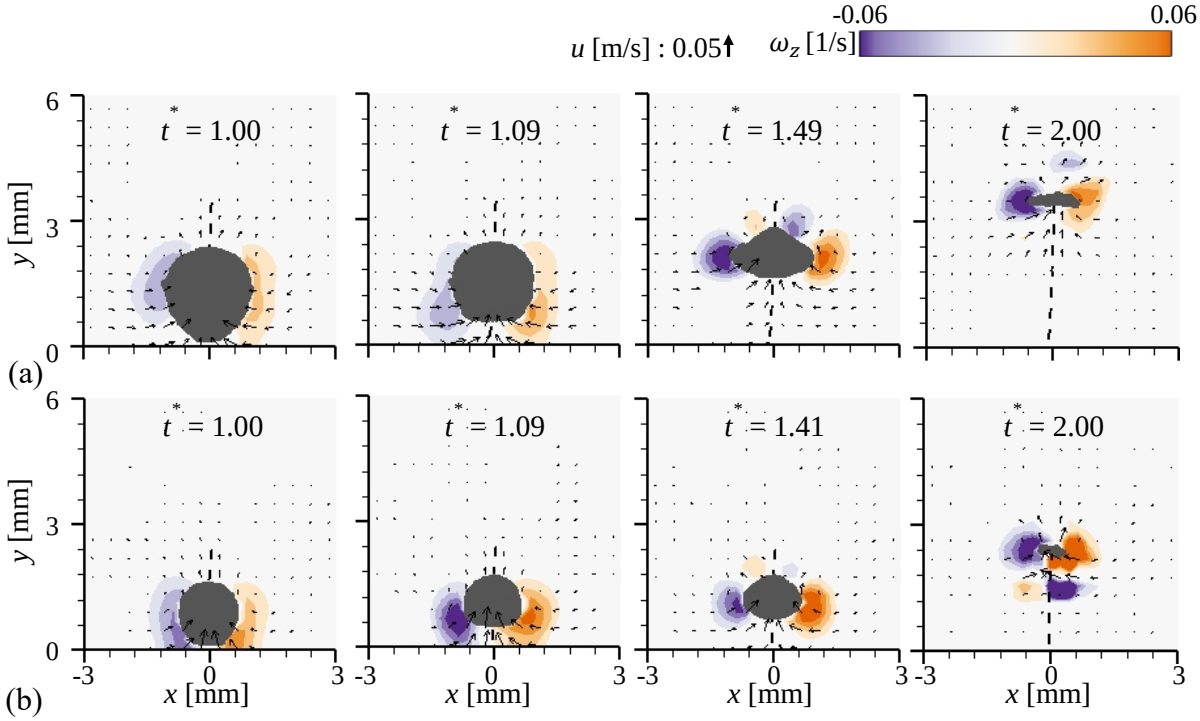

Figure 3.17. Time history of the flow field induced by the rising vapor bubble with (a) ΔT_{sub} = 8℃ and (b) ΔT_{sub} = 15℃. Here, ΔT_{wall} = 4℃ and the dashed line denotes the rising trajectory of the bubble.

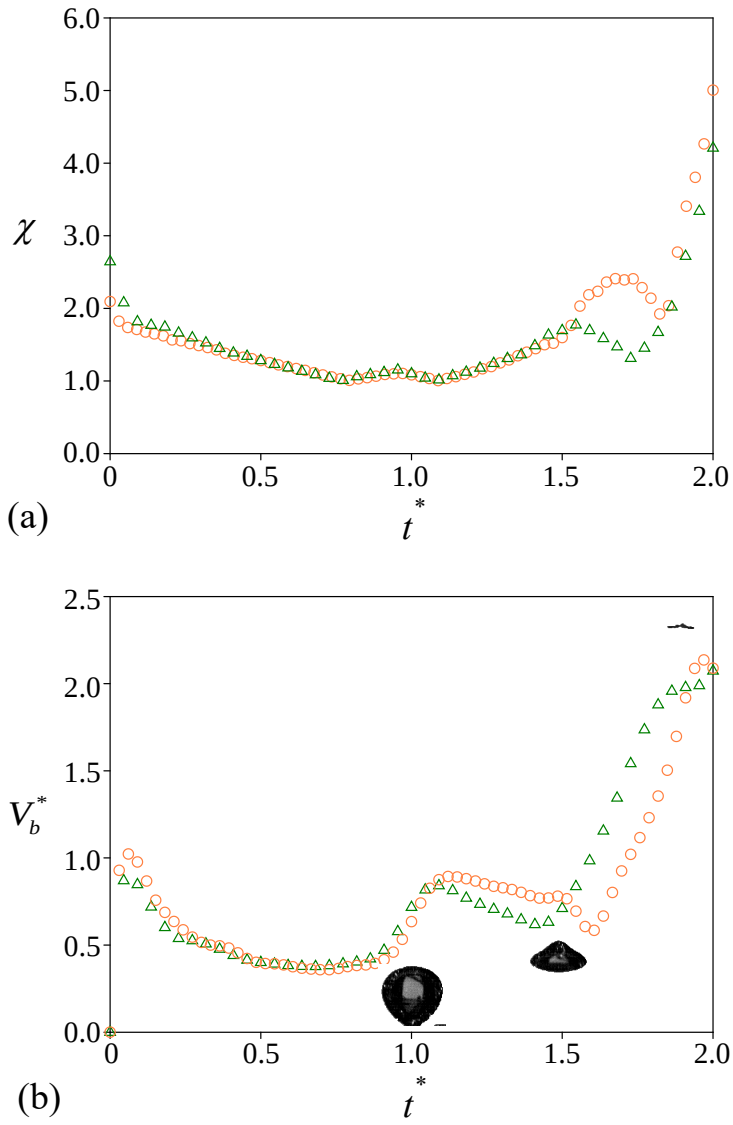

Figure 3.18. Time history of bubble statistics in a highly subcooled conditions: (a) bubble aspect ratio (χ); (b) bubble rising velocity (V_b^*). ○, ΔT_{sub} = 8℃; △, 15℃. Here, ΔT_{wall} = 4℃.

Chapter 4
Conclusion

Experimental investigation for subcooled nucleate pool boiling has been performed to understand the effect of subcooled condition on the dynamics of boiling bubble and corresponding flow field of liquid. As the subcooled temperature grows, both bubble growth time and bubble departure exponentially decay. In higher subcooled condition, the bubble growth rate rapidly declines by means of enhanced condensation. In this study, we developed the bubble growth model in subcooled pool boiling condition by modifying the existing models. The major heat transfer mechanisms (e.g., microlayer evaporation, heat diffusion and condensation) are considered to be superposed for the model, while applying two coefficients to improve the accuracy. Consequently, the present model predicts the trend of bubble growth in both less and highly subcooled conditions. For example, the bubble in a less subcooled condition continuously grows, while the bubble in a highly subcooled condition begins to shrink before departure. Such difference in the bubble growth trend is determined by the competing effects of condensation and heat diffusion after the microlayer is completely depleted.

A vapor bubble rising in a less subcooled water ($\Delta T_{sub} < 8$°C) undergoes a few cycles of significant surface deformation. Depending on the direction of liquid stream induced by bubble deformation, the bubble repeats to be accelerated and decelerated. As the surface tension becomes greater with persistently shrinking bubble, radical transition of bubble structure occurs from flattened oblate ellipsoidal disk to spherical cap shape, producing the asymmetry in bubble

structure and rising path. However, in highly subcooled condition, rising bubble is rapidly condensed and dissipated through less significant surface deformation. Flattened to the most, the bubble completely disappears rising with nearly highest velocity. Bubble induced circulating flow in the wake region of bubble, which is concerned with transient conduction and micro-convection heat transfer, develops larger in less subcooled condition, transferred further from the wall. While the heat and mass transfer induced by single bubble seems more effective in less subcooled condition, examination for time-averaged heat transfer coefficient is still required, as the frequency of bubble departure is greater in highly subcooled condition.

Bibliography

Ahmadi, R., Ueno, T., Okawa, T. Bubble dynamics at boiling incipience in subcooled upward flow boiling. Int. J. Heat Mass Transf. 55 (2012) 488–497.

Asai, A. Application of the nucleation theory to the design of bubble jet printers. Jpn. J. Appl. Phys. 28 (1989) 909–915.

Baltis, C. H. M., van der Geld, C. W. M. Heat transfer mechanisms of a vapour bubble growing at a wall in saturated upward flow. J. Fluid Mech. 771 (2015) 264–302.

Bhaga, D., Weber, M. E. Bubbles in viscous liquids: shapes, wakes and velocities. J. Fluid. Mech. 105 (1981) 61–85.

Chen, Z., Hu, X., Hu, K., Utaka, Y., Mori, S. Measurement of the microlayer characteristics in the whole range of nucleate boiling for water by laser interferometry. Int. J. Heat Mass Transf. 146 (2020) 118856.

Cho, H. J., Wang, E. N. Bubble nucleation, growth, and departure: A new, dynamic understanding. Int. J. Heat and Mass Transf. 145 (2019) 118803.

Colombo, M., Fairweather, M. Prediction of bubble departure in forced convection boiling: A mechanistic model. Int. J. Heat Mass Transf. 85 (2015) 135–146.

Cooper, M. G. The microlayer and bubble growth in nucleate pool boiling. Int. J. Heat Mass Transf. 12 (1969) 915–933.

Cooper, M. G., Lloyd, A. J. P. The microlayer in nucleate pool boiling. Int. J. Heat and Mass Transf. 12 (1969) 895-913.

Demiray, F., Kim, J. Microscale heat transfer measurements during pool boiling of FC-72: effect of subcooling. Int. J. Heat Mass Transf. 47 (2004) 3257-3268.

Duan, X., Phillips, B., McKrell, T., Buongiorno, J. Synchronized high-speed video, infrared thermometry, and particle image velocimetry data for validation of interface-tracking simulations of nucleate boiling phenomena. Exp. Heat Transf. 26 (2013) 169-197.

Ern, P., Risso, F., Fabre, D., Magnaudet, J. Wake-induced oscillatory paths of bodies freely rising or falling in fluids. Annu. Rev. Fluid Mech. 44 (2012) 97-121.

Forster, H. K., Zuber, N. Dynamics of vapor bubbles and boiling heat transfer. Amer. Inst. Chem. Eng. 1 (1955) 531-535.

Gao, M., Zhang, L., Cheng, P., Quan, X. An investigation of microlayer beneath nucleation bubble by laser interferometric method. Int. J. Heat Mass Transf. 57 (2013) 183-189.

Gerardi, C., Buongiorno, J., Hu, L., McKrell, T. Study of bubble growth in water pool boiling through synchronized, infrared thermometry and high-speed video. Int. J. Heat Mass Transf. 53 (2010) 4185-4192.

Goel, P., Nayak, A. K., Kulkarni, P. P., Joshi, J. B. Experimental study on bubble departure characteristics in subcooled nucleate pool boiling. Int. J. Multiphas. Flow 89 (2017) 163-176.

Gong, S., Cheng, P. Lattice Boltzmann simulations for surface wettability effects in saturated pool boiling heat transfer. Int. J. Heat Mass Transf. 85 (2015) 635−646.

Griffith, P. Bubble growth rates in boiling. J. Heat Transf. 80 (1958) 721−727.

Jaikumar, A., Kandlikar, S. G. Pool boiling enhancement through bubble induced convective liquid flow in feeder microchannels. Appl. Phys. Lett. 108 (2016) 041604.

Judd, R. L., Hwang, K. S. A comprehensive model for nucleate pool boiling heat transfer including microlayer evaporation. J. Heat Transf. 98 (1976) 623−629.

Jung, S., Kim, H. An experimental method to simultaneously measure the dynamics and heat transfer associated with a single bubble during nucleate boiling on a horizontal surface. Int. J. Heat Mass Transf. 73 (2014) 365−375.

Jung, S., Kim, H. An experimental study on heat transfer mechanisms in the microlayer using integrated total reflection, laser interferometry and infrared thermometry technique. Heat Transf. Eng. 36 (12) (2015) 1002−1012.

Kays, W. M., Crawford, M. E. Convective Heat and Mass Transfer, 3rd ed., McGraw−Hill, New York, 1993.

Kim, J. Review of nucleate pool boiling bubble heat transfer mechanisms. Int. J. Multiphas. Flow 35 (2009) 1067−1076.

Kim, J., Oh, B. D., Kim, M. H. Experimental study of pool temperature effects on nucleate pool boiling. Int. J. Multiphas. Flow 32 (2006)

208-231.

Kim, M., Lee, J. H., Park, H. Study of bubble-induced turbulence in upward laminar bubbly pipe flows measured with a two-phase particle image velocimetry. Exp. Fluids 57 (2016) 55.

Lawson, N. J., Rudman, M., Guerra, A., Liow, J. L. Experimental and numerical comparisons of the break-up of a large bubble. Exp. Fluids 26 (1999) 524-534.

Lee, J., Park, H. Bubble dynamics and bubble-induced agitation in the homogeneous bubble-swarm past a circular cylinder at small to moderate void fractions. Phys. Rev. Fluids 5 (2020) 054304.

Lee, J., Park, H. Wake structures behind an oscillating bubble rising close to a vertical wall. Int. J. Multiphas. Flow 91 (2017) 225-242.

Lin, L., Ponnappan, R. Heat transfer characteristics of spray cooling in a closed loop. Int. J. Heat Mass Transf. 46 (2003) 3737-3746.

Lindken, R., Merzkirch, W. A novel PIV technique for measurements in multiphase flows and its application to two-phase bubbly flows. Exp. Fluids 33 (2002) 814-825.

Maeng, H., Park, H. An experimental study on the heat transfer by a single bubble wake rising near a vertical heated wall. Int. J. Heat Mass Transf. 165 (2021) 120590.

Mikic, B. B., Rohsenow, W. M. A new correlation of pool-boiling data including the effect of heating surface characteristics. J. Heat Transf. 9 (1969) 245-250.

Narayan, S., Srivastava, A., Singh, S. Rainbow schlieren-based

investigation of heat transfer mechanisms during isolated nucleate pool boiling phenomenon: Effect of superheat levels. Int. J. Heat Mass Transf. 120 (2018) 127–143.

Plesset, M. S., Zwick, S. A. The growth of vapor bubbles in superheated liquids. J. Appl. Phys. 25 (1954) 493–500.

Prosperetti, A. Vapor bubbles. Annu. Rev. Fluid Mech. 49 (2017) 221–248.

Raj, S., Pathak, M., Khan, M. K. An analytical model for predicting growth rate and departure diameter of a bubble in subcooled flow boiling. Int. J. Heat Mass Transf. 109 (2017) 470–481.

Ranz, W. E., Marshall, W. R. Evaporation from drops, part I. Chem. Eng. Prog. 48 (1952) 141–146.

Sato, Y., Niceno, B. A depletable micro–layer model for nucleate pool boiling. J. Compt. Phys. 300 (2015) 20–52.

Sato, Y., Niceno, B. Nucleate boiling simulations using the interface tracking method: Boiling regime from discrete bubble to vapor mushroom region. Int. J. Heat Mass Transf. 105 (2017) 505–524.

Shoji, M. Studies of boiling chaos: a review. Int. J. Heat Mass Transf. 47 (2004) 1105–1128.

Tolubinsky, V. I., Kostanchuk, D. M. Vapour bubbles growth rate and heat transfer intensity at subcooled water boiling. In: Proceedings of the 4th international Heat Transfer Conference, (1970).

Tolubinsky, V. I., Ostrovsky, J. N. On the mechanism of boiling heat transfer (vapour bubbles growth rate in the process of boiling of liquids, solutions, and binary mixtures). Int. J. Heat Mass Transf.

9 (1966) 1463-1470.

Tong, L. S., Tang, Y. S. Boiling heat transfer and two-phase flow, Taylor and Francis, 1997.

Tripathi, M. K., Sahu, K. C., Govindarajan, R. Dynamics of an initially spherical bubble rising in quiescent liquid. Nat. Comm. 6 (2015) 6268.

Tu, J. Y., Yeoh, G. H. On numerical modelling of low-pressure subcooled boiling flows. Int. J. Heat and Mass Transf. 45 (2002) 1197-1209.

Utaka, Y., Kashiwabara, Y., Ozaki, M. Microlayer structure in nucleate boiling of water and ethanol at atmospheric pressure. Int. J. Heat Mass Transf. 57 (2013) 222-230.

van Stralen, S. J. D. The mechanism of nucleate boiling in pure liquids and in binary mixtures-part I. Int. J. Heat Mass Transf. 9 (1966) 995-1020.

van Stralen, S. J. D., Sohal, M. S., Cole, R., Sluyter, W. M. Bubble growth rates in pure and binary systems: Combined effect of relaxation and evaporation microlayers. Int. J. Heat Mass Transf. 18 (1975) 453-467.

Warrier, G. R., Basu, N., Dhir, V. K. Interfacial heat transfer during subcooled flow boiling. Int. J. Heat Mass Transf. 45 (2002) 3947-3959.

Yabuki, T., Nakabeppu, O. Heat transfer mechanisms in isolated bubble boiling of water observed with MEMS sensor. Int. J. Heat Mass Transf. 76 (2014) 286-297.

Zuber, N. The dynamics of vapor bubbles in nonuniform temperature fields. Int. J. Heat and Mass Transf. 2 (1961) 83-98.

국문 초록

본 연구에서는 과냉 조건의 풀비등현상에서 발생하는 증기 기포의 거동과 그에 따른 주변 액체의 유동장을 실험적으로 분석하였다. 기포의 시간에 따른 변화 (성장, 분리, 상승, 그리고 소멸)는 과냉 온도에 따라 다른 특징을 보인다. 과냉 조건 (ΔT_{sub} = 2−15°C)을 변수로 하여, 기포 구조의 변화와 주위에 유도되는 액체의 유동장을 초고속카메라를 이용한 이상−입자유동영상계를 활용하여 동시에 측정하였다. 과냉 온도가 커질수록, 기포가 열판에서 분리될 때의 크기 (d_d)가 기하급수적으로 작아지며, 분리되는 순간까지 걸리는 시간 (t_g) 또한 유사한 경향성을 보인다. 과냉 온도가 비교적 낮은 조건 (ΔT_{sub} < 8°C)에서는 기포가 성장하여 분리되기 직전까지 지속적으로 성장하는 반면, 과냉 온도가 비교적 큰 환경 ($\Delta T_{sub} \geq$ 8°C)에서는 가열면에서 분리되기 전부터 기포가 응축 열전달로 인하여 크기가 줄어들기 시작한다. 본 연구에서는 기포 성장에 영향을 미치는 열전달 메커니즘들을 기반으로, 과냉 조건에서의 풀비등 기포 성장 모델을 개발하였다. 과냉 온도가 낮은 조건 (ΔT_{sub} < 8°C)에서 성장하여 분리된 기포 (2.5−3.1mm)는 수직으로 상승하며 천천히 응축하고, 유체 관성력의 지배적인 영향으로 인해 표면 구조의 변형이 강하게 발생한다. 이러한 표면 구조의 변형이 반복적으로 나타나며, 기포의 상승 속도와 종횡비가 등락을 거듭한다. 반면, 과냉 온도가 높은 조건 ($\Delta T_{sub} \geq$ 8°C)에서는 기포 (1.5−2.2mm)가 벽면에서 분리된 이후에 매우 빠르게 응축하여 소멸한다. 이때, 기포는 분리 이후에 지속적으로 가속되며, 완전히 응축하여 소멸하기 직전에 표면 구조가 가장 납작해지는 경향을 보인다. 상승하는 기포 주위로 발달하는 와류 구조 또한 과냉 온도가 낮은 조건에서 더 강하게 발달하며, 가열면으로부터 더 멀리 전달됨을 발견하였다.

핵심어 : 과냉 풀비등, 비등 열전달, 기포류 유동, 기포 거동, 입자 이미지 속도 측정

학번 : 2019-23495